

12-2021

Synthesis and Characterization of Centrifugally Spun Molybdenum-Based Nanomaterials for Lithium-Ion Batteries

Ramiro Gonzalez Jr.
The University of Texas Rio Grande Valley

Follow this and additional works at: <https://scholarworks.utrgv.edu/etd>



Part of the [Mechanical Engineering Commons](#)

Recommended Citation

Gonzalez, Ramiro Jr., "Synthesis and Characterization of Centrifugally Spun Molybdenum-Based Nanomaterials for Lithium-Ion Batteries" (2021). *Theses and Dissertations*. 879.
<https://scholarworks.utrgv.edu/etd/879>

This Thesis is brought to you for free and open access by ScholarWorks @ UTRGV. It has been accepted for inclusion in Theses and Dissertations by an authorized administrator of ScholarWorks @ UTRGV. For more information, please contact justin.white@utrgv.edu, william.flores01@utrgv.edu.

SYNTHESIS AND CHARACTERIZATION OF CENTRIFUGALLY SPUN MOLYBDENUM-
BASED NANOMATERIALS FOR LITHIUM-ION BATTERIES

A Thesis

by

RAMIRO GONZALEZ, JR.

Submitted in Partial Fulfilment of the
Requirements for the Degree of
MASTER OF SCIENCE IN ENGINEERING

Major Subject: Mechanical Engineering

The University of Texas Rio Grande Valley

December 2021

SYNTHESIS AND CHARACTERIZATION OF CENTRIFUGALLY SPUN MOLYBDENUM-
BASED NANOMATERIALS FOR LITHIUM-ION BATTERIES

A Thesis
by
RAMIR GONZALEZ, JR.

COMMITTEE MEMBERS

Dr. Mataz Alcoutlabi
Chair of Committee

Dr. Javier Ortega
Committee Member

Dr. Maysam Pournik
Committee Member

December 2021

Copyright 2021 Ramiro Gonzalez

All Rights Reserved

ABSTRACT

Gonzalez Jr., Ramiro, Synthesis and Characterization of Centrifugally Spun Molybdenum Based Nanomaterials for Lithium-ion Batteries. Master of Science in Engineering (MSE), December 2021 55 pp, 2 tables, 19 figures, references, 15 titles

The work presented in this thesis focuses on the processing and development of transition metal compound composite fibers as anode materials for rechargeable lithium-ion batteries (LIBs). Among the transition metal compounds, molybdenum compounds have risen as promising candidates of advanced electrode materials, in view of their natural abundance, virtuous mechanical/thermal stability, rich chemistry, high theoretical specific capacity, and multiple oxidation states of Mo. The current work reports synthesize MoO_2/C and MoO_3/C composite fibers drawn from centrifugal spun ammonium molybdate/PAN precursor fibers, followed by a thermal treatment stabilizing in air and calcination under argon atmosphere. The weight ratios of (MoO_x , $2 \leq x \leq 3$) were controlled to illustrate the ideal high performing activities and stable concentration. The calcination of ammonium molybdate/PAN precursor fibers develop MoO_3 material which reached a specific capacity of 1052 mAhg^{-1} at 80 cycles, while ending at 1004 mAhg^{-1} after 100 cycles. The synthesized material outperformed commercial nanoscale MoO_3 delivering a charge capacity of 836 mAhg^{-1} after 70 cycles.

This work is then followed by the electrical performance of molybdenum disulfide (MoS_2) coated with graphene oxide (GO) and reduced graphene oxide (rGO) obtained through a facile hydrothermal process involving ammonium tetra thiomolybdate and graphite. The use of an

exfoliated multilayer and few-layer structures of GO with MoS₂ inherently delivered increased specific capacity, prolonged stability, and improved electrochemical performance of the MoS₂/GO composite electrode. Various concentrations of MoS₂ to GO were used to promote the performance of the electrode, while altering calcination temperatures directly affected the morphology and the structural stability of the composite anode. MoS₂/rGO exhibited good electrochemical performance after prolonged charge/discharge cycles, delivering discharge and charge capacities of 1068 mAhg⁻¹ and 641 mAhg⁻¹, at the first cycle, respectively, where 88% of its capacity was retained after 100 cycles. The outstanding electrochemical performance of the MoS₂/rGO composites is attributed to the exfoliation of GO network, dominating performances for all concentrations, making the composite electrode a promising anode material for high performance LIBs.

DEDICATION

The completion of my master's degree would not have been possible without the love and support from my family. Thank you to my father Ramiro Gonzalez, and my mother Maria Gonzalez, who encourage me day by day to pursue further in life from a young age. Thank you for listening and giving me words of advice when times became tough. Thank you for giving me the opportunity to chase after this dream, the dream you both wanted me to achieve ever since we moved to this country. Thank you for believing in me and giving me this and many other blessings. I love you both a lot and thank you in bringing me up to be a better individual.

To my girlfriend, for her love and affection, for always continuing to reassure me that I could achieve this. Thank you for being my rock and for all the wonderful memories that you allowed me to be a part of; Whatever comes my way, I will hold your hand and know it will be okay.

To my siblings, Hector, Ezequiel, Martin, and Victoria, thank you for always making me laugh and leaving me with a smile; I am forever thankful for always cheering me on throughout this journey and to show you we can achieve great things.

ACKNOWLEDGMENTS

A special thank you to Dr. Mataz Alcoutlabi, chair of my thesis committee for all his mentoring and patience, for always teaching us the importance of research and hard work. Many thanks to my thesis committee members: Dr. Javier Ortega and Dr. Maysam Pournik, as well as Dr. Padilla and Dr. Lozano for their guidance throughout the years.

I would also like to thank my research group, thank you guys for the talks we had, thank you for having me look forward to going to work every day, thank you for listening to any questions I had and providing feedback, thank for the multitude of discussion we had allowing us to all grow and become better every day. Thank you for allowing me to be your mentor, all the laughs, and being able to call you family. I truly hope we stay lifelong friends.

TABLE OF CONTENTS

	PAGE
ABSTRACT.....	iii
DEDICATION.....	v
ACKNOWLEDGMENTS.....	vi
TABLE OF CONTENTS.....	vii
LIST OF TABLES.....	ix
LIST OF FIGURES.....	x
CHAPTER I. INTRODUCTION.....	1
CHAPTER II. LITERATURE REVIEW.....	3
2.1 Energy Storage Technologies.....	3
2.2 Lithium-ion Batteries.....	4
2.3 Anode Materials.....	11
2.3.1 Nanostructured Anodes.....	12
2.3.2 Graphene Composites.....	13
2.3.3 Metal Oxides.....	15
2.3.4 Molybdenum Oxides.....	16
2.3.5 Molybdenum Disulfides.....	18
2.4 Forcespinning.....	19
CHAPTER III. EXPERIMENTAL PROCEDURE.....	22
3.1 Material selection.....	22
3.1.1 Preparation of MoS ₂ /GO and MoS ₂ /rGO composites.....	22
3.1.2 Preparation of MoO ₂ /C and MoO ₃ /C composite fibers.....	23
CHAPTER IV. RESULTS AND DISCUSSION.....	24
4.1 Morphology and Characterization.....	24
4.1.1 MoO ₂ /C and MoO ₃ /C Composite Fibers.....	24
4.1.2 MoS ₂ /GO and MoS ₂ /rGO Composites.....	27
4.2 Electrochemical Results.....	30

4.2.1 MoO ₂ /C and MoO ₃ /C Composite Fiber Anodes	30
4.2.2 MoS ₂ /GO and MoS ₂ /rGO Composite Anodes	36
CHAPTER V. CONCLUSION.....	42
CHAPTER VI. FUTURE WORK	44
REFERENCES	45
APPENDIX.....	50
BIOGRAPHICAL SKETCH	55

LIST OF TABLES

	PAGE
Table 1. Impedance parameters values from the equivalent circuit model.....	36
Table 2. EIS parameters values from the equivalent circuit model fitting.	41

LIST OF FIGURES

	PAGE
Figure 1. Schematic of a LiCoO_2 cathode, electrolyte, separator, and graphite anode electrode.	6
Figure 2 schematic of the working mechanisms during charge and discharge of a lib.	7
Figure 3. The SEI layer inside the LIB.	10
Figure 4. 2032 coin-cell assembly	11
Figure 5. Forcespinning cyclone with spun fibers.	20
Figure 6. SEM and edax of cnf (a, b), 60 wt.% MoO_2/C (c, d) and MoO_3/C (e, f).	24
Figure 7. XRD patterns for the 60% MoO_3/C (A) and 60% MoO_2/C (B).	26
Figure 8. TGA thermograms of CNF and various weight concentrations of MoO_2/C	27
Figure 9. Powder XRD patterns collected for GO and MoS_2/GO hybrid material.	28
Figure 10. XPS spectra for MoS_2/GO composite material composites.	29
Figure 11. SEM of MoS_2 (a,b,c), MoS_2/GO (d,e,f) and MoS_2/rGO composites.	30
Figure 12. CV on various weight percentages of MoO_2/C composites (a-d) and MoO_3/C (e).	32
Figure 13. Charge-discharge performance of 60 wt.% MoO_2/C (a) and MoO_3/C (b) composites. ..	33
Figure 14. Cycle performance and coulombic efficiency MoO_2/C and MoO_3/C composites	33
Figure 15. EIS measurements on various weight of MoO_2/C composites.	35
Figure 16. CV curves of (a) MoS_2 , (b) hybrid MoS_2/GO , and (c) MoS_2/rGO composites.	37
Figure 17. Charge-discharge performance of (a) MoS_2/GO and (b) MoS_2/rGO composites.	39
Figure 18. CP and coulombic efficiency on (a, b) MoS_2/GO and (c, d) MoS_2/rGO	40
Figure 19. EIS of (a) MoS_2/GO and (b) MoS_2/rGO	41

CHAPTER I

INTRODUCTION

The lifeline of today's modern technological world consists of a portable power supply. One issue by renewable energy is storage. Electricity can be generated by renewable sources, but the production by these sources do not coincide with the electrical demand of the population (e.g., solar energy, wind energy) [1]. Batteries serve as an alternative solution for customers with high electricity demands. Currently, AMBRI batteries are attempting to store the energy gathered from wind and solar efficiency to power cities and remote areas similarly to Tesla's home battery (Powerwall) and utility-scale system, the Powerpack. There are a multiple of different batteries for different applications, but rechargeable lithium-ion batteries (LIBs) are currently dominant energy storage devices and have been ever since their development and commercialization by Sony in the early 1900s. The LIB was based on electrochemical potential of an electrochemical series, utilizing lithium as the source of electrons. The element lithium has the highest tendency to lose an electron since one electron can be found in its outer-most shell. Currently, LIBs compared to other types of electrochemical storage devices such as other rechargeable/secondary batteries (e.g., Lead Acid, Ni-Cd, Ni-MH) and supercapacitors or electrochemistry energy conversion devices (e.g., fuel cells) offer a broader range of voltage operations and greater volumetric and gravimetric energy densities. Their superior energy performance, reduced size and weight serves as a better alternative

for a convenient power source. Alternative rechargeable alkali metal-ion (e.g., potassium-ion, aluminum-ion and sodium-ion) batteries serve as a substitute for the lithium available threatened assuming the demand surpasses the available quantity due to the current rapid increase of LIB. It is said that LIBs may also overshadow gasoline power technologies, just as Tesla is currently attempting to do [2-8]. The electrical and hybrid electric vehicles (EV/HEV) are currently revolutionizing the automotive industry by introducing battery technology. Vehicles are being presented to induction motors, slowly minimizing the usage of internal combustion engines due to their advantage in almost all engineering characteristics (e.g., speed control, initial torque, etc.). The fundamental building blocks derived from a single affordable and efficient battery cell due to the current advancements in technology for LIBs. To take the induction motors to the next level, the power supply requires further investigation. After the improvement of the cathode having a multitude to select from and introduction of key additives in electrolytes during the late 20th century and early 21st century, the anode electrode has yet to make a breakthrough in LIBs. The graphite which has recently replaced hard carbons still pends improvement. Anode materials (e.g., being cost efficient and sustainable. The idea is to have fewer atoms to store lithium, thus having a smaller volume of materials storing the same energy as graphite. The graphite anode is limited and cannot meet the increasing energy demand in energy density, operational reliability and system integration. The work presented on this thesis experiments with nanoscale materials and structures to further meet the energy demands in the modern society. Precursors and synthesize materials are also investigated [9-15].

CHAPTER II

LITERATURE REVIEW

2.1 ENERGY STORAGE TECHNOLOGIES

The question of how-to firm renewables, that is ensuring there's energy in demand no matter the time of day or weather, is one of the biggest challenges in industry. As mentioned, a green route of massive sources of energy flows around in nature (e.g., solar, wind and wave). Over the past decade, prices for solar panels and wind farms have reach an all-time low, and with future developments emerging, renewable energy will continue to minimize in cost. These alternative renewable sources provide an eco-friendly route minimizing environmental issues (e.g., global warming) and limited fossil fuels in terms of electrical energy storage (EES). Some flaws surface when examining the whole schematic of renewable sources as electricity produces during a rise in demand. Limitations in renewable energy-based power generating systems comprise of intermittent and non-controllable factors forming major hurdles. Applications vary and include stationary energy sources, transport vehicles, or portable devices to provide suitable EES. The core option present during this time are LIBs, but due to the current price range of the battery, even with its significant cost decline, grid-scale application task is limited. Conveniently, the EES a LIB promotes results in flexibility in power and energy densities, low cycle life, being efficient through

long cycles, while providing pollution-free forms of operation. [16-18] Currently, dozens of alternatives for storage technologies have blossom in the early stages. Some of these alternatives presently being explored include flow aqueous batteries, which store liquid electrolyte in external tanks causing a separation between the energy from the electrolyte and the actual source of power generation. Companies like Primus Power, ESS Inc., form energy, and AMBRI introduced flow batteries to the market, but being in their early stages, combined with their severe cost and manufacturing challenges, can act as barricades towards them from being able to be priced competitively against LIBs. These types of batteries remain incapable of obtaining energy storage capacity over long periods of time. Other alternative includes mechanical storage technologies like pump hydro and compressed air. Energy Vault, which are gravity-based systems, require a huge area to operate, diminishing them from being placed around vast cities. The energy density is very low, thus chemical-based storage mediums are still a huge advantage in LIBs. Antora energy develops electricity storage through heating on carbon blocks and when needed the heat will convert back into electrical energy through a reversible mechanism occurring in a heat engine. [19-21] Other energy storage solutions include chemical storage involving hydrogen fuel cells (biofuels). As it is seen, all alternative EES systems establish positive and negative attributes involving cost of storage, storage efficiency and power liable on the application. These options remain to satisfy requirements, most common being cost, to appeal to a global scale demand.

2.2 LITHIUM-ION BATTERIES

All batteries have the common basic components: current collectors, a negative electrode called the anode, a positive electrode called the cathode, separator, and a chemical layer called an

electrolyte. The high energy storage systems LIBs possess is due mainly to their low atomic weight and redox potential [$E_0(\text{Li}/\text{Li}^+ = -3.04 \text{ V})$]. [22] A LIB working principle consist of three materials: one that wants electrons, another which wants to give up electrons and a pathway for the buildup of charge to neutralize. The intercalation storage mechanism enables the shuttling of lithium continuously repeating back and forth as time progresses between the positive and negative host electrode materials. A cathode is the positive electrode from which a current departs a polarized power supply. As it is known, electrons have a negative charge, so the movement of the electrons is opposite to the conventional current flow. In LIBs, the cathode is the positive terminal since that is where the current flows out of the system. This outward current is carried out by positive ions moving from the electrolyte to the positive cathode due to the discharge state of the battery, also known as reduction reaction. As this process is occurring, an alternative reaction called oxidation, or loss of electrons, is happening opposite to that of the cathode during the discharge state. The role of the reactions alternates as a battery is charging. Most typical commercial cathodes being used consists of metal oxides that can accommodate lithium. The most common being lithium cobalt oxide (LiCoO_2), lithium iron phosphate (LiFePO_4) or lithium manganese oxide (LiMn_2O_4). The cathode is the lithium source of the battery, meaning that it provides the lithium ions (Li-ion) for the oxidation and reduction reactions that occur while a battery is charging and discharging. Currently, graphite is the current dominant commercialized negative anode electrode having a theoretical capacity of 372 mAhg^{-1} . The current collectors are depended on two major criteria: excellent conductivity to aid the cathode and anode in distributing the electrodes and potential stability. The layered-oxide cathode is coated onto a current collector consisting of aluminum foil. The working potentials for aluminum falls anywhere from 3-4.7 V, while the graphite is mounted onto the copper current collector being stable at a potential below 3 V.

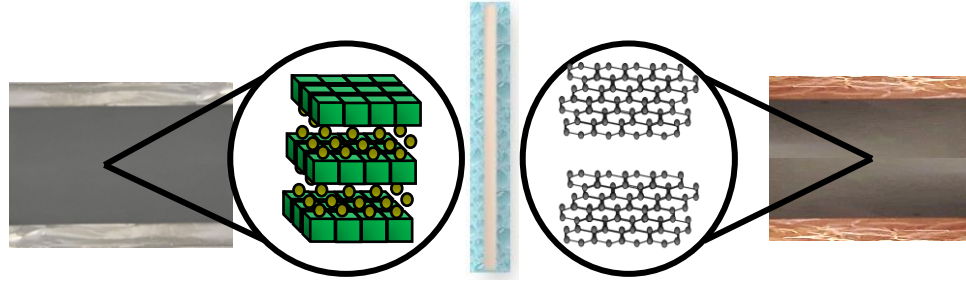
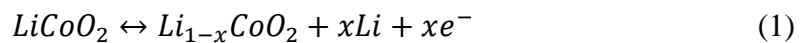


Figure 1. Schematic of a LiCoO_2 cathode, electrolyte, separator, and graphite anode electrode.

The mechanism that occurs in graphite is called intercalation, in which the lithium fits in between graphite sheets and sits there not taking part of the chemical reaction. This phenomenon occurs due to the anode material being considered a storage medium for Li-ion. Although this is the case, the current technology has developed broader preparation and modification of alternative materials for higher capacity meaning it will be able to store more lithium. In electrochemistry, the reduction, or gain of electrons, and oxidation, loss of electrons, operations are known as redox reactions that continuously occur while a battery is charging, meaning a certain voltage has been applied, and discharging, meaning an external circuit has been connected. During the charge/discharge profiles, as the electrons flow through the external circuit, delithiation and lithiation occur simultaneously. When a power source is applied, the positive side of the power source will attract and remove electrons from the Li-ions from the lithium metal oxides of the cathodes through a working mechanism called delithiation. The electrons will then be attracted to the current collector that will travel to the negative terminal, thus causing the Li-ion to follow. This process is known as lithiation or intercalation of the Li-ions to the graphite layer. This chemical reaction is considered unstable. The lithium ions are shuffled between the cathode and anode during charge/discharge profiles as follows:



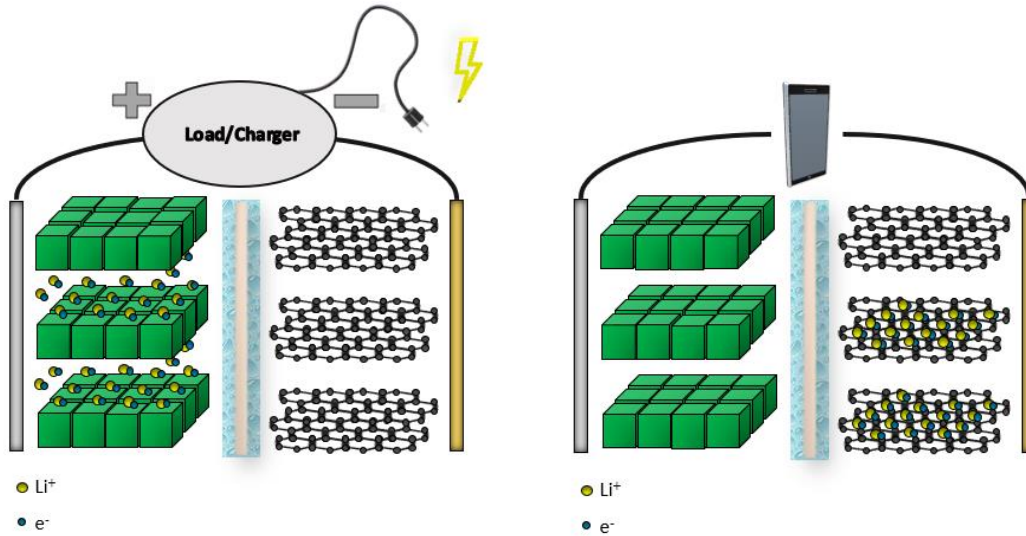


Figure 2 schematic of the working mechanisms during charge and discharge of a lib.

The electrolyte acts as a guard allowing only the Li-ion to travel between the electrodes allowing lithium diffusion. The electrons are not allowed, having them travel through the external circuit to reach the graphite layer. Therefore, electrolyte can be considered an ionically conductive and electronically insulating medium. Liquid electrolyte solutions are based on volume ratios composed of carbonate organic solvents (e.g., ethylene carbonate (EC), dimethyl carbonate (DMC), diethyl carbonate (DEC) and ethyl methyl carbonate (EMC), including inorganic lithium salt (e.g., $LiPF_6$) dissolved in the mixture with various other additives. Most commonly, organic electrolytes consist of ethylene carbonate (EC) and dimethyl carbonate (DMC) solvent blends due to their ionic conductivity and high stability at higher voltages. The solvents are typically mixed because some may be beneficial due to having much lower boiling points giving good low temperature performances while other may form good passivating layers on the negative electrode. The current concern with the current organic liquid electrolytes is their flammability due to internal

degradation over time. Typically, a separator is placed between the cathode and anode. The separator is an insulating physical layer placed between the cathode and anode that is permeable for the Li-ion due to the micro porosity thin film of the structure typically consisting of ceramics or polymers. With the surge in high energy demand in this current era, energy storage systems continue to evolve, but having higher energy density materials, erupts safety problems (e.g., thermal runaway (TR) due to low thermal stability causing thermal abuse within the battery. Before getting to TR, a mechanical abuse, followed by an electrical abuse, which leads to the thermal abuse gradually arose from a negative chain reaction. When a battery is performing, if the temperature rises due to some abnormal condition (e.g., separator collapsing or shrinking), the liquid electrolyte will dry up leading to an internal short circuit, typically due to overcharging continuously demanding too much current, between the anode and cathode. This may lead to some common features of TR, which include a battery experiencing smoke, which may lead to a fire or even an explosion linked with battery operations. [23] Separators containing a multilayer structure (e.g., polyethylene (PE) – polypropylene (PP)) have been known to play a vital role in LIB safety conditions and TR, by having PE melt and fill up multiple pores, thus increasing the cell resistance to terminate cell operation. [24] Safety protection agents, including overcharge protectors and fire-retardant additive (e.g. MOILES), have been electrolyte additive investigated to avoid TR.

When a power source is placed, the electrons will be forced to travel and find themselves in the anode material with the Li-ion simultaneously following during the initial charge and discharge cycle. The Li-ion will be at the graphite surface intercalation, thus charging the LIB. The lithiated graphite, which is graphite with lithium inside, is very reactive when exposed to electrolyte. On the cathode, the lithium transition metal oxide with the missing lithium is also very reactive. This unstable state causes both electrodes to react with the electrolyte solution, which is a major

problem due to possibly degradation if electrons encounter it. Incredibly, the solvent molecules in the electrolyte cover the Li-ion deriving a solid layer once reaching the graphite material. The decomposition reaction between the graphite and the solvent molecules that cover the Li-ion produce a passive film called the solid-electrolyte interface (SEI) limiting further reactions by avoiding sudden degradation. The SEI serves as a shield as it prevents the electrons from further contact with the electrolyte, preventing diffusion of the materials and stabilizing the electrodes. The layer is a heterogenous mass comprising of inorganic and organic components. Plays a crucial role in the long term cyclability where a passivation layer form allowing the redox reactions to continue.

As the SEI layer is forming, it slows down the reactions occurring between the lithium in the graphite and the electrolyte solution. When a LIB is tested, the first initial cycle will demonstrate the phenomenon observing an irreversible capacity deterioration. This is due to some of the lithium that transfer to the graphite layer getting trapped by some components of the SEI, including lithium oxides, lithium fluoride, lithium carbonate or oligomers. This analogy is examined throughout each charge/discharge profile of the LIB since fractures occur within the SEI layer resulting in parasitic reactions (e.g., dendrites, electron tunneling) happening across the electrolyte. The parasitic reactions are most notably cause by materials experiencing an enormous volume change (e.g., silicon alloys) as cycles progress causing so much SEI growth to occur. This in terms, can cause delamination from the electrical contact, having particles merely sitting in the overall assembly, not contributing to the LIB. As mentioned, dendrites are also cause for the failure modes that can occur on the surface of the LIB separator leading up to a direct contact between the cathode and anode minimizing the life cycle. Another disastrous flaw causing degradation includes the SEI film not forming properly during the first cycle, causing a slight number of

electrons found in the graphite to tunnel through during discharging. Some porous areas in the SEI layer permit the solvent molecules that are present in the electrolyte to attract to the electrons causing another reaction. Once the solvent molecules react, another SEI film is form causing an accelerated thickening of the layer while having more electrolyte and L consumption. To combat this, excellent SEI layer composition and structure have been generated due to slower formation current density being generated only in the first cycle to improve LIBs efficiency and stability. [25]

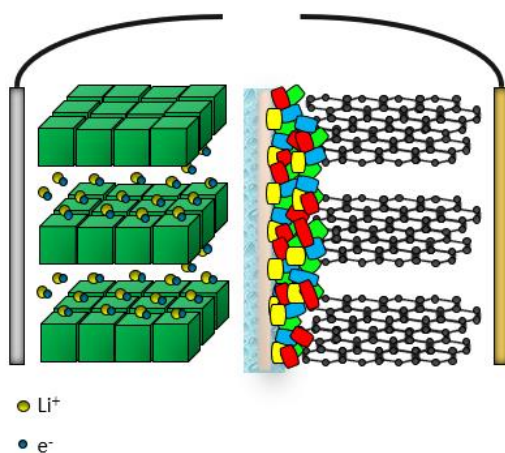


Figure 3. The SEI layer inside the LIB.

The electrochemical performance of the samples was studied using coin type (2032) half cells. The assembling process was carried out in a glovebox (Mbraun, USA) filled with laboratory grade level argon having a concentration of H₂O and O₂ < 0.5 ppm. The flexible composite anodes were directly used as binder-free working electrode (anode) in Li-ion half cells while a Lithium metal foil was used as the counter electrode (cathode). 20 mm-size glass microfibers served as separators, a stainless-steel spring will ensure good electrical contact between the components once the lithium-half cell is sealed, while a stainless-steel spacer acts as a flat rigid current collector for the cathode. The electrolyte used for the samples were 1M LiPF₆ solution in ethylene carbonate

(EC)/dimethyl carbonate (DMC) (1:1 v/v). The electrochemical performance was examined by galvanostatic charge (lithium insertion) and discharge (lithium extraction) experiments using a LANHE Battery Testing System (CT2001A) instrument over a voltage range of 0.01-3.00 V vs. Li/Li⁺. The charge/ discharge capacities were calculated based on the mass of the flexible nanofiber anode. A Biologic Science Instrument performed cyclic voltammetry (CV) at a scan rate of 0.1 mVs⁻¹ ranging between 0.05 and 3.00 V. Electrochemical impedance spectroscopy (EIS) measurements were carried out over a frequency range from 1 kHz and 0.05 Hz using AUTOLAB PGSTAT 128 N, Metrohm.

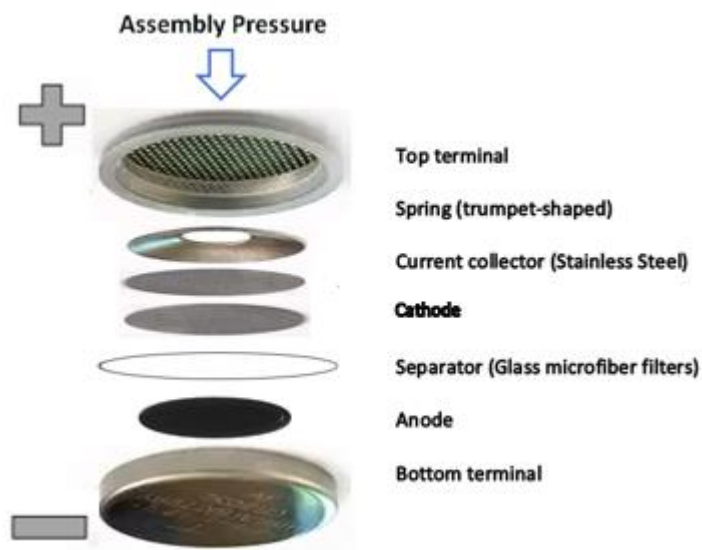


Figure 4. 2032 coin-cell assembly

2.3 ANODE MATERIALS

One of the vital components of a LIB is the anode electrode which is the negative terminal of the system. Constituted of graphite, a carbonaceous material, the anode is the storage

mechanism of lithium. The graphite anode is limited and cannot adequately meet the increasing energy demand in energy density, operational reliability and system integration. For this apparent reason, a proper ideal design of the hybrid anode to properly promote the existing anode is widely considered. Multitudes of materials and morphologic structures have challenged the present anode, but the graphite anode remains. An ideal hybrid anode should promote an enormous amount of Li-ions to be store during the charging (lithiation) phase, while also deliberately releasing those Li-ions during discharge (delithiation) back into the system throughout the reduction-oxidation (redox) chemical reactions during long-extensive cycles. While this is taking place, the initial cycle should experience slight irreversible capacity though still delivering a suitable SEI film layer on the surface of the anode material advocating safety for future preventable incidents. This in terms will minimize extensive elevated volume alterations being more efficient and maintaining that efficiency while undoubtedly possessing an adequate low-cost material and structure that can ostensibly promote high-energy sustainability.

2.3.1 NANOSTRUCTURED ANODES

The performance of LIBs has gradually increased, almost doubling in capacity due to the graphite replacing hard carbons and by introducing new additives with the LiCoO_2 electrolyte. The idea of finding an alternative anode material to trap higher energy has opened a broader spectrum of the potential the LIB's EES system own. This trend is due to the anode electrode possessing a high influence on the performance of the LIB. To further improvise the anode materials (e.g., transition metal sulfides/oxides, alloys, alternative carbon-based materials), techniques to alter the structure at a nanoscale have been studied.[31]

A material at a nanostructure comprises of special properties, both chemical and physical, benefiting the electrode due to the change in size and morphology. A material's structure is considered nano if one dimension of the system falls below a range of 100 nanometers (nm), in an aggregate or agglomerate state. Due to the particle size at a nanoscale, an increment is seen on the number of atoms lying near or on the surface, thus causing the electrochemical reactivity more versatile compare to bulk materials. The nanomaterials comprise of countless forms (e.g., 0, 1, 2 and 3D) and nanostructured shapes (e.g., nanowires, nano sphere, nanocrystals, etc.). The multitude of advantages include having large electrode/electrolyte contact area, short path length for Li-ion diffusion while having high mechanical stiffness and shorter lithium insertion/extraction. With advantageous benefits, the nanoscale materials also come with some unwanted reactions. These reactions may occur due to the higher surface energies and larger surface areas, but if a proper SEI film is form, the probability of them occurring is minimize. Other reactions reside from low tap densities, higher inter-particle resistances and thermodynamic instability from which nanomaterials are known to demonstrate [32, 33, 34].

2.3.2 GRAPHENE COMPOSITES

Graphite remains dominant as the anode electrode particularly due to being sustainable, abundant, and overall practical due to its low cost. Initially, hard carbons were utilized as anode materials in the early 20th century, but the demand and pressure from device manufacturers led to the introduction of graphite being one of several changes to the LIB, maintaining a carbon-based material as the anode electrode. Carbons possess several perks over metal oxides because they exhibit, both higher specific charges and more negative redox potentials, while having an

advantage over alloys in cycling performance by processing excellent dimensional stability. [27] Carbonaceous materials, being non-graphitic (hard carbons) possesses the ability to produce more superior capacities than that of graphite due to the aid of their disordered structure. This in terms promotes more Li-ions to be inserted, but a vast disadvantage revolves around the enormous irreversible capacity initially experience. This phenomenon revolves around the SEI layer being highly influence by the large surface area hard carbons have to offer due to the material being exposed to air. More diminished volumetric capacities also arose for being less dense from the structure.[28] The transition in the carbon-based anode electrode gave rise to graphitic (soft carbon) alternatives. Being first study in the 1980s, graphite is the most stable allotrope of carbon having the ability of requiring six carbon atoms to accommodate one Li-ions in its layered gap (0.335 nm) crystal structure sheets giving a theoretical capacity of 372 mAhg^{-1} . It is composed of a monolayer of sp^2 hybridized carbon graphene sheets, which can be stacked (i.e., α -hexagonal or β -rhombohedral) patterns, resembling a honeycomb crystal lattice kept together by van der Waals bonding forces being acquired in two forms (i.e., natural or synthetic). [29, 30] When a battery is charge, Li-ions intercalate between an interstitial site of layers of graphite while being reverse during discharge, causing minimal structure expansion as repeated intercalation/deintercalation go on. The slight volume change experience allows for continuous charge capacity thus being suitable for commercial usage in terms of efficiency sacrificing capacity. The intercalation/deintercalation process can be viewed in Equation 2.

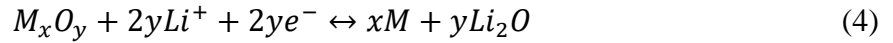
2.3.3 METAL OXIDES

Transition-metal oxides (e.g., single, binary, ternary metal oxide, etc.) have been proposed as a beneficial alternative possibility for the continuous search of an electrode material to satisfy the desired demand of LIB's EES systems. The chemical and physical properties derived from the metal-containing compounds in the form of oxides promote highly reversible capacities in elevated working voltages making them ideal choice as an electrode material candidate. Metal oxides offer distinct structures (e.g., tunneled) compared to the intercalation mechanism the current graphite layered carbon-based structure anode hold. The tunnel structure materials (e.g., $\text{Li}_4\text{Ti}_5\text{O}_{12}$ or TiO_2) regularly establish low specific capacity values due to electrons during the insertion reaction being less than one per Li through an insertion mechanism. As mentioned, graphite exhibits a layered structure. Multiple metal oxides (e.g., iron oxides, cobalt oxides, molybdenum oxides, etc.) share similar structures to graphite having more potential to store Li^+ demonstrating redox properties during insertion of Li^+ . Displacement metal oxide material's concept is to displace one metal from an intermetallic compound during a Li-alloy reaction mechanism. The reaction mechanism can demonstrate a solid-solution reaction and addition reaction if a phase transformation takes place. During alloying, the Li is inserted into the crystal structure and extracted during dealloying. Tin(IV) oxide (SnO_2) is the most common metal oxide demonstrating a combination of conversion and alloying mechanisms [35-37]. The three reaction mechanisms dependent on the structure of the metal oxides can be seen below:

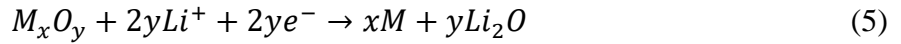
Insertion reaction mechanism:



Conversion reaction mechanism:



Li-alloy reaction mechanism:



2.3.4 MOLYBDENUM OXIDES

Molybdenum dioxide (MoO₂) and Molybdenum trioxide (MoO₃) possess high theoretical capacities, 830 mAhg⁻¹ and 1111 mAhg⁻¹ respectively. Layered transitioned metal oxides, like molybdenum oxides, contain similar structure to that of graphite making them a prime candidate material for usage while storing Li through the conversion reactions. Advantages of utilizing conversion-based electrodes include better rate capabilities, safe working potentials and as mentioned high specific capacity (800-1200 mAhg⁻¹). The considerably higher capacity of MoO₂ than graphite derives from the ability to support more Li⁺ by hosting 4 Li atoms per formula unit, while MoO₃ can accommodate 6 Li⁺. A weakness of molybdenum oxides is faced during the charge/discharge profiles displaying poor cyclic stability. [38] The Li diffusion undergone during conversion reaction leads to an excessive volume expansion owed to low retention. Typically, anomalous reversible capacity is demonstrated before a substantial amount of capacity degradation can be seen after deep cycles.

MoO₂ and MoO₃ are among the common metal oxide states for Mo-based compounds used as anodes for LIBs and SIBs due to their immense theoretical specific capacity at 838 mAh g⁻¹ and 1117 mAh g⁻¹, respectively [38-40]. MoS₂ favors a structure resemblance to graphite, while supplying a larger interlayer space and offering a high theoretical specific capacity of 670 mAhg⁻¹ [21, 22]. However, these conversion-type electrodes suffer from massive volume expansion and poor electronic conductivity during the alloying/dealloying with Li⁺. To overcome this, a conductive medium is applied in the form of carbonaceous materials to enhance the electrochemical performance. Shan et al. reported 3D nanoarchitecture composites consisting of MoO₂ decorated in graphene oxide (GO) obtained through a hydrothermal route. The MoO₂/GO composite electrode exhibited a discharge capacity of 817 mAhg⁻¹ at 100 mA g⁻¹ and keeping a specific capacity up to of 524 mAh g⁻¹ after 30 cycles. On the other hand, at 500 mA g⁻¹, a capacity of 507 mAh g⁻¹ was obtained during the discharge cycle and retained roughly at 310 mAh g⁻¹ after prolonged charge/diaschrge cycles [41]. Kowsalya et al. reported porous MoO₂/graphene microspheres which ran up to 1405 and 1375 mAh g⁻¹ for initial discharge and charge capacities at 10 C rate with minimal capacity fading, while having the MoO₂ experienced an activation process, permitting an increase in capacity after just 10 cycles [42]. Also, Xueqian et al. synthesized MoS₂@C nanotube composite via a hydrothermal sulfuration process achieving discharge and charge capacities of 1327 and 1221 mAhg⁻¹ at 0.1C rate with an initial Coulombic efficiency of 92%, even obtaining 850 mAhg⁻¹ at 5C during rate performance [43]. Sanmu et al. fabricated coaxial TiO₂/MoO₃@CNFs and MoO₃@CNFs through electrospinning and subsequent annealing, in which both electrodes exhibited a long-term cycling stability up to 300 cycles at 1000 mA g⁻¹. The MoO₃@CNFs had a capacity retention of 42.3%, while the TiO₂/MoO₃@CNFs affirmed a reversible capacity of 561 mAh g⁻¹ with a capacity retention of 70.8% [44-45].

2.3.5 MOLYBDENUM DISULFIDES

Molybdenum disulfide (MoS_2) is among the common transition metal compounds used as anodes for LIB due to their theoretical specific capacity at 670 mAhg^{-1} based on four moles of Li^+ insertion per mole of MoS_2 and most notably favoring a structure resemblance to graphite supplying a larger interlayer space of 0.615 nm to 0.355 nm, respectively [46]. The 2D layered structure is composed of hexagonal S-Mo-S layers stacked together through notable weak van der Waals forces favoring facile intercalation among the Li^+ with minimal increase in volume. Though, the practical application of MoS_2 conversion-type material in LIBs has been plagued by their high surface energy triggering irreversible structural degradation through restacking, and aggregation experiences of the layers leading up to poor capacity retention and rate capabilities [47]. To evade this, conductive medium support such as, graphene, graphene oxide and reduced graphene oxide promote long cycle life and acceptable chemical stability making them ideal for the MoS_2 semiconductor [48]. For example, Yuan et al. synthesized hierarchical MoS_2 -rGO nanosheets via L-Cysteine-assisted hydrothermal process followed by a thermal annealing treatment process achieving 1010 mAhg^{-1} at $100 \text{ mA}g^{-1}$ rate, even obtaining 700 mAhg^{-1} at $1000 \text{ mA}g^{-1}$ during rate performance [49]. Also, Zhang et al. fabricated $\text{MoO}_2@/\text{MoS}_2/\text{rGO}$ core-shell structure composites through a facile sulfuration and hydrothermal treatment derived from MoO_3 . As LIB anode electrodes, $\text{MoO}_2@/\text{MoS}_2/\text{rGO}$ provided a reversible capacity of 833 mAh g^{-1} with a capacity retention of 80.6% at $200 \text{ mA}g^{-1}$ attributed to the optimized interface and low specific surface area [50].

2.4 FORCESPINNING

Lithium-ion batteries (LIBs) are currently the dominant energy storage device that has become the lifeline of today's modern world. Although this is the case, the research done to further improve anode electrode has open new opportunities to take the performance of the LIB to the next level. As it has been understood, graphite is currently the material utilize in anode electrodes since it has shown to be stable over long periods of time. This is due to the low volume change being experience during the charge/discharge profiles. Slurry current electrode, which consist of active material coated on copper foil are the current way in which LIBs are produced. Electro-spun carbonized fibers have been introduced as an alternative way of producing an anode. This proposition is great, but a fresher alternative called force-spinning using centrifugal forces has been widely used to develop nanofibers. This method has not only cause fibers to be produced at a more rapid scale, but it has also overcome the present limitations the electrospinning method encounters and has brought fibers down to the nanometer scale. This simple and flexible system has opened new doors to the electrochemistry world in terms of energy storage. A composite carbon fiber and graphite slurry current collector are both carbon-based materials. These two anodes are the starting point (control) of any LIB in terms of research before modifying the electrode's structure. More interesting properties can be investigated at the nanometer scale not only on the fibers, but also nanomaterials, compared to the slurry electrode which only focuses on the nanomaterial.



Figure 5. Forcespinning cyclone with spun fibers.

Extensive attention has revolved around LIBs and their contribution to the environmental pollution. Nano fibers introduce an environmental friendliness, besides the materials being utilized on the carbon-based anode. The fibers being water-soluble are even more eco-friendly. The downfall of these fibers derives from the heat treatment being processed to develop the amorphous carbon for the anode to be conductive as it performs. The carbon fibers tend to shrink tremendously, so further work is needed to introduce water soluble solutions. Another parameter to consider is the overall weight of the anode. When examining the nano/microfibers, the anode exhibits a smaller mass than that of a slurry electrode. The current collect (copper foil) is simply inactive mass and volume in the assembly of the battery. Although this is the case, the copper current collector serves as a conductor and has electrochemical stability. For copper, that range for stability is at lower ranges that can be up to 3 volts while oxidating. Thinner and lighter foils have been investigated to resolve the gravimetric and volumetric energy densities. With this in mind, cost-efficiency is sacrificed, thus not making it ideal for commercial usage. In previous

experimental work, carbon fibers do demonstrate lower electronic conductivity than copper which may limit their use. One major setback for copper current collectors is fibers have demonstrated increasing the surface area to volume ratio due to the adoption of nano and microstructures and flexibility, which minimize the overall volume. Chemical reactions don't only depend on the material properties since the reduction of the electrode thickness has been shown to improve capacity. Increasing the surface area to volume ratio has also been known to reduce the temperature the battery is experiencing while cycling. This is crucial when the battery is being tested under different temperatures depending on the application. When examining both carbon-based anodes, typical cycle performance is around 300 to 400 mAh/g. The introduction of metal oxides or alloy materials is highly considered due to how lithium reacts during the charge/discharge profiles. For example, lithium in its pure form is very reactive, but when its part of a metal oxide it becomes quite stable. Having the introduction of these materials, all containing their pros and cons, allows the anode electrode to achieve higher capacity to achieve higher energy densities [51-57].

CHAPTER III

EXPERIMENTAL PROCEDURE

3.1 MATERIAL SELECTION

N, N-Dimethyl Formamide (DMF) was obtained from Fisher Scientific (USA), Graphite & Carbon Black, Super P Conductive were purchased from Alfa Aesar while Polyacrylonitrile (PAN) with an average Mw of 150,000, ammonium tetrathiomolybdate $[(\text{NH}_4)_2\text{MoS}_4]$ and ammonium molybdate $[(\text{NH}_4)_6\text{Mo}_7\text{O}_{24}\cdot 4\text{H}_2\text{O}]$ were all purchased from Sigma-Aldrich (USA). Deionized (DI) water was used throughout the synthesis process.

3.1.1 PREPARATION OF MoS_2/GO AND MoS_2/RGO COMPOSITES

The synthesis of the materials was performed in three phases. The first phase was the preparation of the graphene oxide using a modified Hummer's method. The resulting GO particles was collected using centrifugation, washed with acetone, and dried overnight at 85°C. The second step in the MoS_2/GO preparation is the synthesis of the $(\text{NH}_4)_2\text{MoS}_4$ precursor to produce the MoS_2 materials. Ammonium tetrathiomolybdate (ATM) were synthesized using a previously described method. The product was collected by cooling in an ice bath, filter, and washed using

cold isopropyl alcohol. GO mixture containing a specific mass of either CoCl_2 or NiCl_2 . Subsequently, the promoter, ATM, and GO will be sonicated at room temperature for 1 hour. After sonication, the sample will be collected by vacuum filtration, washed with acetone, and dried. The material will be converted to the catalytic phase in a tube furnace at 350°C for 1h under a 90% Ar: 10% H_2 gas mixture flowing at 10 mL/min. The catalytic sample will be cooled to room temperature naturally and then collected and characterized.

3.1.2 PREPARATION OF MoO_2/C AND MoO_3/C COMPOSITE FIBERS

The MoO_2/C composite fibers were prepared by centrifugal spinning (Cyclone L-1000 M, FibeRio Technology) an ammonium molybdate/PAN precursor solution followed by stabilization of the precursor fibers in air at 280°C for 3 h and then by calcination at 700°C for 3 h in an argon atmosphere (heat rate of $3^\circ\text{C}/\text{min}$). MoO_3/C was stabilized at 400°C for 3 h. The solutions were formulated by dissolving 12 wt.% PAN in DMF solvent containing the ammonium molybdate precursor. The concentration of ammonium was incremented each time by 20 wt.%, concluding at 80 wt.% for MoO_2/PAN and MoO_3/PAN fibrous mats. The precursor fibers were then prepared through centrifugal spinning by injecting 2 mL of the precursor solution into the spinneret. The quality of fibers was dependent on a variety of parameters: solution viscosity, rotational speed of the spinneret, surrounding temperature and humidity. The spinneret rotational speed and spinning time were augmented and placed at 7500-9,000 rpm for 20-45 s, respectively. Fibrous mats of MoO_2/PAN were collected with a desired thickness and were then dried in a vacuum oven for 12 h at 60°C .

CHAPTER IV

RESULTS AND DISCUSSION

4.1 MORPHOLOGY AND CHARACTERIZATION

4.1.1 MoO_2/C AND MoO_3/C COMPOSITE FIBERS

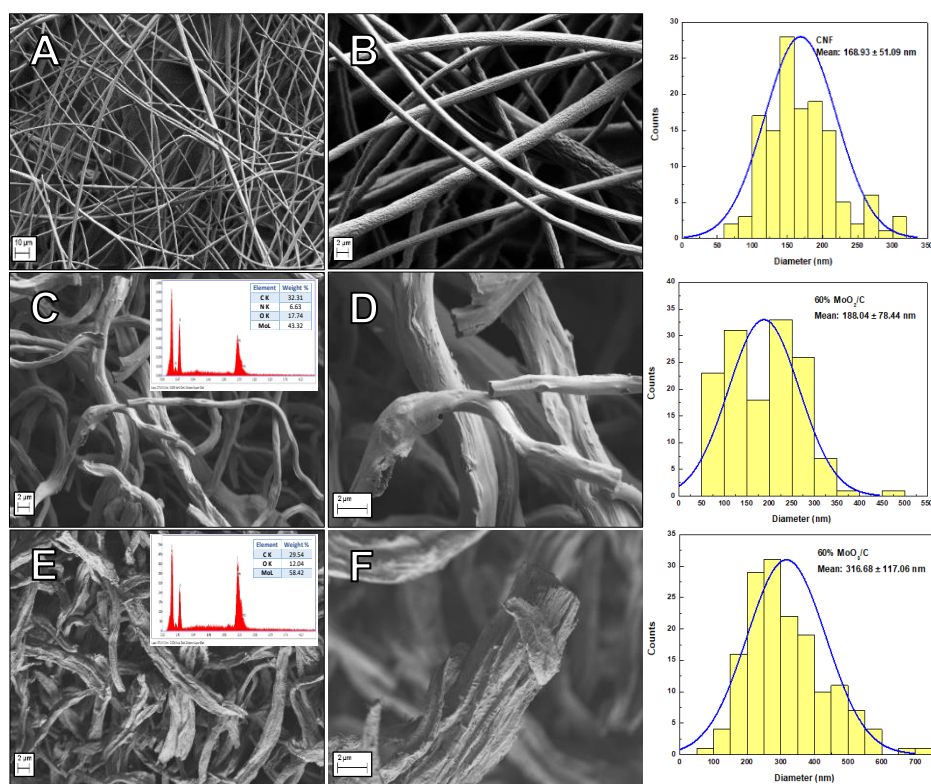


Figure 6. SEM and EDAX of cnf (a, b), 60 wt.% moO_2/c (c, d) and moO_3/c (e, f).

To study the surface morphology and structure of the MoO_3/C and MoO_2/C composite fibers, SEM images were displayed in Figure 6. The carbonized fibers demonstrate a smooth surface (Figure 1a), while the embedded material formed a rough texture throughout the morphology. The addition of the MoO_x material can be viewed in the carbonized samples demonstrating a “clot” within the fibers to form MoO_3/C and MoO_2/C . Histograms confirmed that all the thin composite fibers were at a nanoscale with an average fiber diameter of 180-261 nm. The EDAX spectrum based on the target sample surfaces validated the presence of the MoO_x material. The elemental compositions of the CNF composites are composed of elements Mo, O, C and N on the MoO_3 and MoO_2 electrodes. Furthermore, the element composition distribution of each element was similar in each concentration, confirming the successful synthesis of the MoO_3/C and MoO_2/C composites.

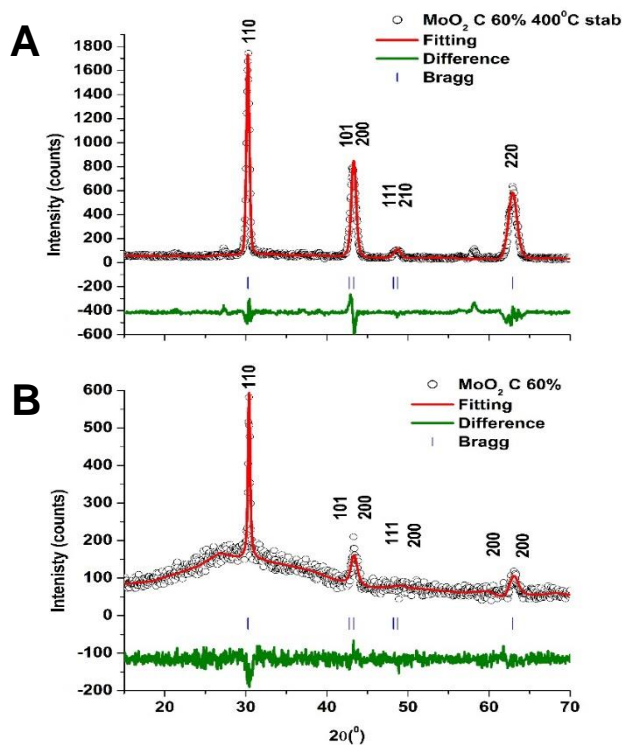


Figure 7. XRD patterns for the 60% MoO₃/C (A) and 60% MoO₂/C (B).

Thermogravimetric Analysis (TGA) was conducted under an air atmosphere to determine the MoO_x loading in the composites compared to the CNF composites (Figure 8). Initial temperatures presented indications of minor weight loss due to surface bound moisture around 100 °C still present even after calcination. Additional degradation attributed in connection with the low carbonization temperature. Uncarbonized species of PAN present at the CNF were chemically unstable oxidizing while demonstrating slight thermal stability up to 390 °C having an onset degradation temperature ranging from 500-520 °C for MoO_x/C composites [38, 39]. All MoO_x/C fiber composites experience an atmospheric reaction at 390 °C, increasing the mass up to 95 wt.% where MoO₂ oxidized to MoO₃ [3]. The CNF control determined 4.6 wt.% resin in the composite structure attributed to polymer impurities and graphitized carbon.

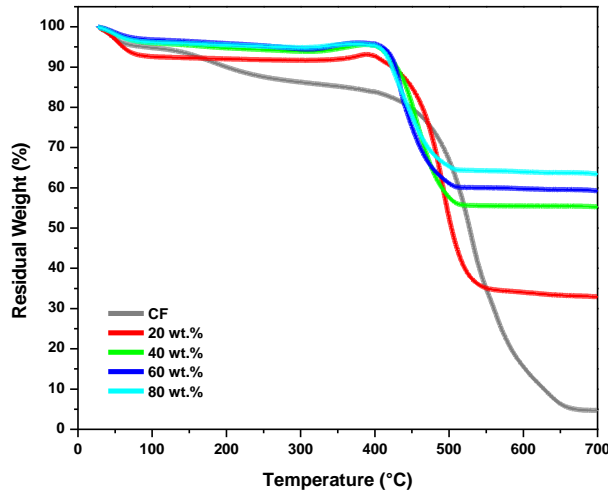


Figure 8. TGA thermograms of CNF and various weight concentrations of MoO₂/C.

4.1.2 MoS₂/GO AND MoS₂/RGO COMPOSITES

The crystal structure of the GO and MoS₂/GO materials was characterized by XRD, where the diffraction pattern for the GO shows two diffraction peaks which are the 001 for GO and the 002 for graphite (Figure 9). The results indicate that a small amount of stacking in the graphite layers is present in the sample after oxidation and separation using Hummer's method. The diffraction pattern for MoS₂/GO shows a very diffuse diffraction plane at 17 in 2θ which is the 002-diffraction plane of MoS₂. The extremely low intensity of the peak indicates a very low stacking in the c-axis direction for MoS₂. In fact, the MoS₂ diffraction plane has shifted to 9 degrees in 2θ, which is indicative of intercalation and expansion on the c-axis of the crystal as it has been reported in the literature [refs]. The XRD data also indicate that a reduction of the GO has occurred to produce rGO while the absence of the 001-diffraction plane in the hybrid material and the presence of the Graphite 002-diffraction plane were located at 31.2° in 2θ. [58]

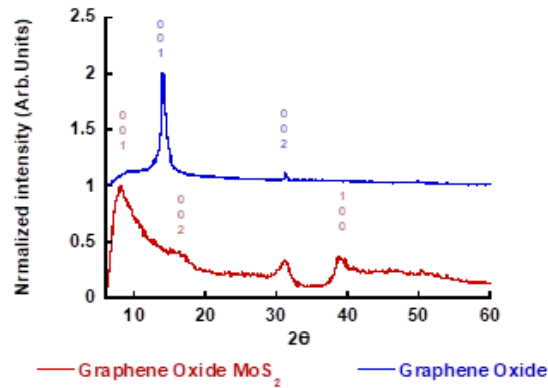


Figure 9. Powder XRD patterns collected for GO and MoS₂/GO hybrid material.

Figure 10 A shows the presence of 2 peaks at 284.2 eV and 285.0 eV which are indicative of sp² C and sp³ C. These two peaks observed at 284.2 and 285 eV are seen in the XPS spectrum of graphene and graphite. The XPS data of carbon does not show the presence of oxidized carbon indicating that a reduction of the GO has occurred to produce rGO, which confirms the interpretation of the XRD data. Figure 10 B shows the XPS spectrum for the Mo 3d region. There are three main peaks and one minor peak. The main peaks are located at 226 eV, 229.0 eV, and 232.15 eV, which are associated with the overlap of the sulfur 2S spectrum, The Mo3d and Mo3/5d peaks are consistent with those reported previously in the literature on the XPS data of MoS₂. respectively . The minor peak located at 234.8 indicated that the presence of a small amount of Mo⁶⁺ is present in the sample. Figure 10 C shows S 1P XPS spectrum for the sample. Two major and one minor peak is observed in the XPS spectrum at 163.0, 161.822, and 168.16 eV. The main peaks are indicative of the MoS₂ compound. The small peak confirms the presence of a very small amount of oxidized sulfur in the sample. Finally, the O2S spectrum is shown in Figure 10 D, which shows a low intensity indicating a low amount of oxygen species are present and curve consists of two peaks at 531.3 and 533.3 eV. These peaks can be linked to the presence of presence of S-O and metal-oxygen bonds, which corroborates the XPS collected from the regions.

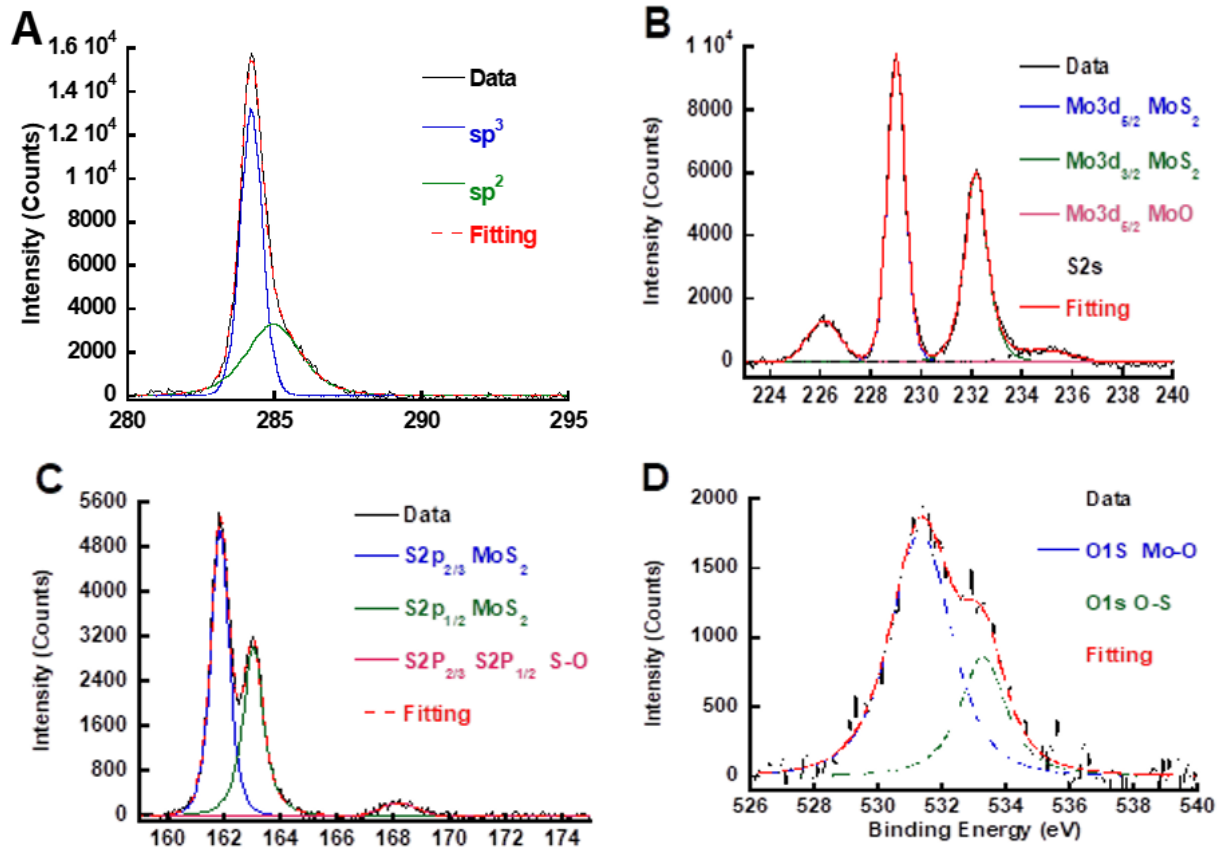


Figure 10. XPS spectra for mos₂/go composite material composites.

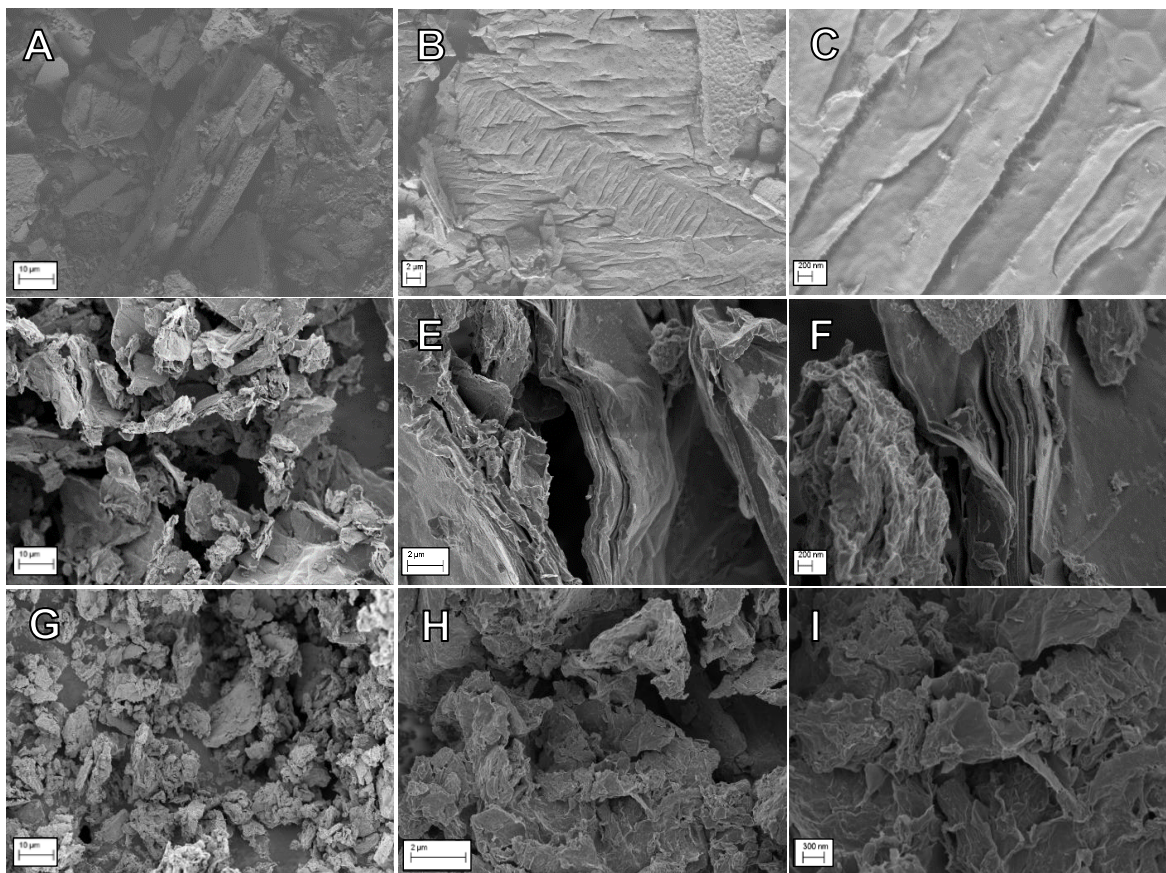


Figure 11. SEM of mos2 (a,b,c),mos2/go (d,e,f) and mos2/rgo composites.

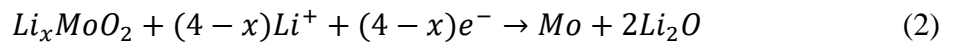
4.2 ELECTROCHEMICAL RESULTS

4.2.1 MoO_2/C AND MoO_3/C COMPOSITE FIBER ANODES

To understand the interaction process of Li^+ with the MoO_2/C and MoO_3/C fiber composites, cyclic voltammetry (CV) measurements were taken for the initial four cycles. The potential window range between 0.05-3.0V (vs Li^+/Li) at a scan rate of 0.2 mVs^{-1} is shown in Figure 12. On the opening cathodic peak for all concentrations, MoO_2 and MoO_3 exhibits two reduction peaks at 1.44 V and 1.71. Similarly, two visible oxidation peaks at 1.26 V and 1.54 V

can be seen throughout the anodic peak on subsequent cycles, where the oxidation of Mo^0 to Mo^{+4} and Mo^{+6} occurs while having the decomposition of Li_2O . The intensified redox pair of 1.44 V/1.26 V and 1.71 V/1.54 V attribute to the reversible phase transitions of Li_xMoO_2 with MoO_2 and Li_xMoO_3 with MoO_3 lattices altering between monoclinic to the orthorhombic to the monoclinic phase due to Li^+ intercalation (discharge) and de-intercalation (charge) [Eqs. 1, 4]. The unchanged redox pair defines a strong stability and reversibility for Li^+ reactions due to minimal change shown on subsequent cycles. A dwarf-size peak at 0.32 V signifies a conversion reaction from MoO_2 and MoO_3 to metallic Mo particles embedded in the Li_2O matrix [Eqs. 2, 5]. The Mo partially alloys/de-alloys close to the theoretical limit of Li_xMoO_2 ($\sim 838 \text{ mAh g}^{-1}$) and Li_xMoO_3 ($\sim 1117 \text{ mAh g}^{-1}$). Additionally, from the ion diffusion and phase change, a broad reduction peak at 0.66 V is attributed to the formation of the solid electrolyte interphase (SEI) derived from the irreversible decomposition of the electrolyte on the electrode surface. The anodic peaks undertook on a conversion of O to Li_2O and Li^+ intercalation [Eqs. 3, 6]. The anodic and cathodic peaks become more evident, as the concentration of MoO_2 enhances. The three reaction mechanisms for MoO_x , ($2 \leq x \leq 3$) can be seen below:

MoO₂



MoO₃



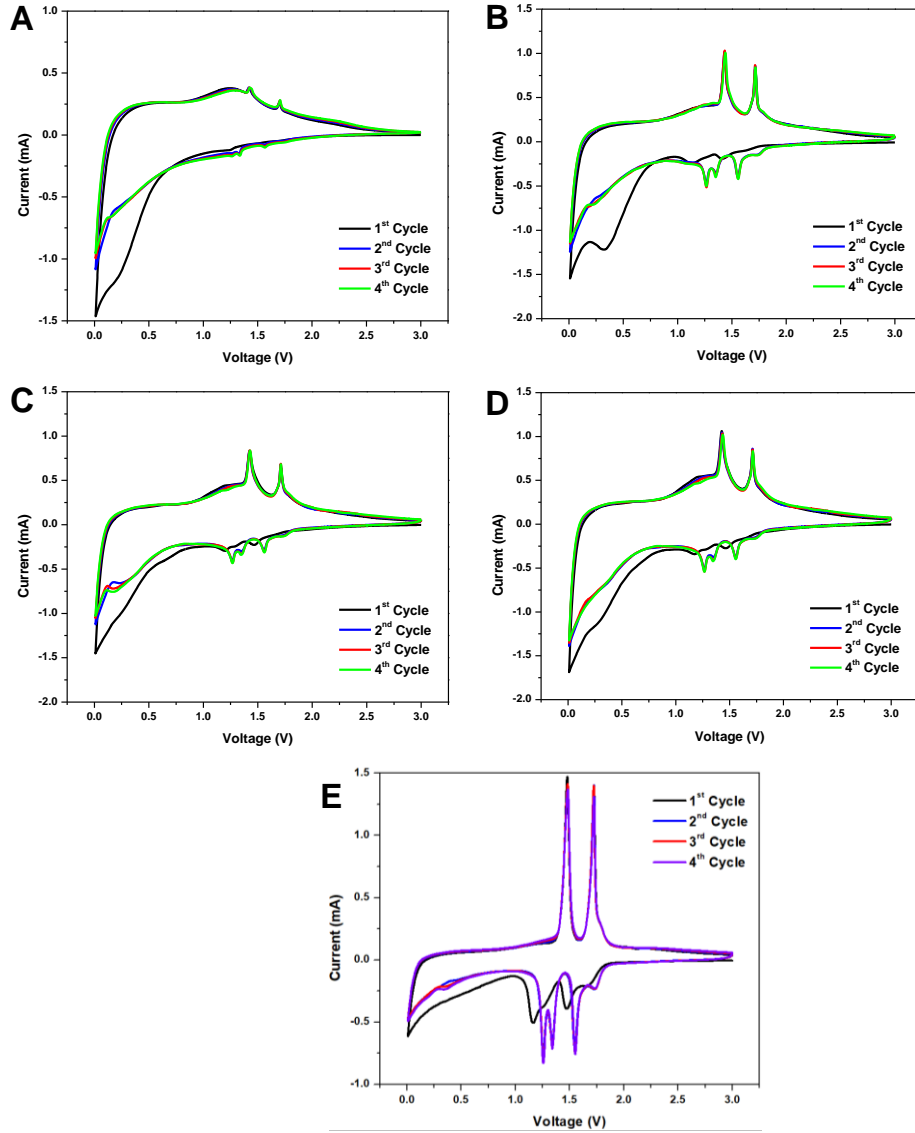
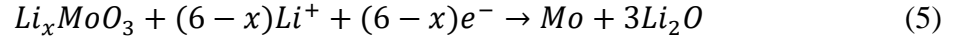


Figure 12. CV on various weight percentages of moo₂/c composites (a-d) and moo₃/c (e).

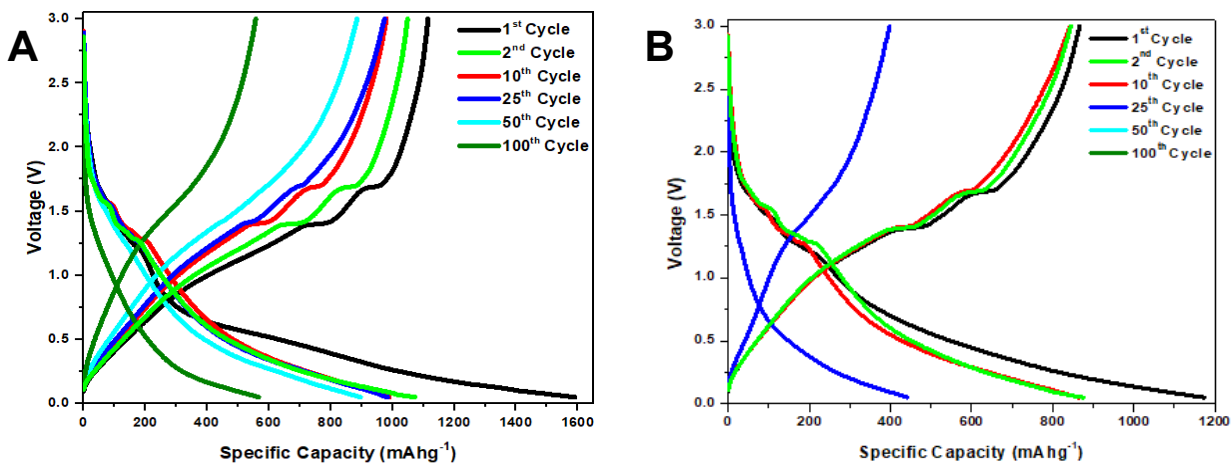


Figure 13. Charge-discharge performance of 60 wt.% MoO_2/C (a) and MoO_3/C (b) composites.

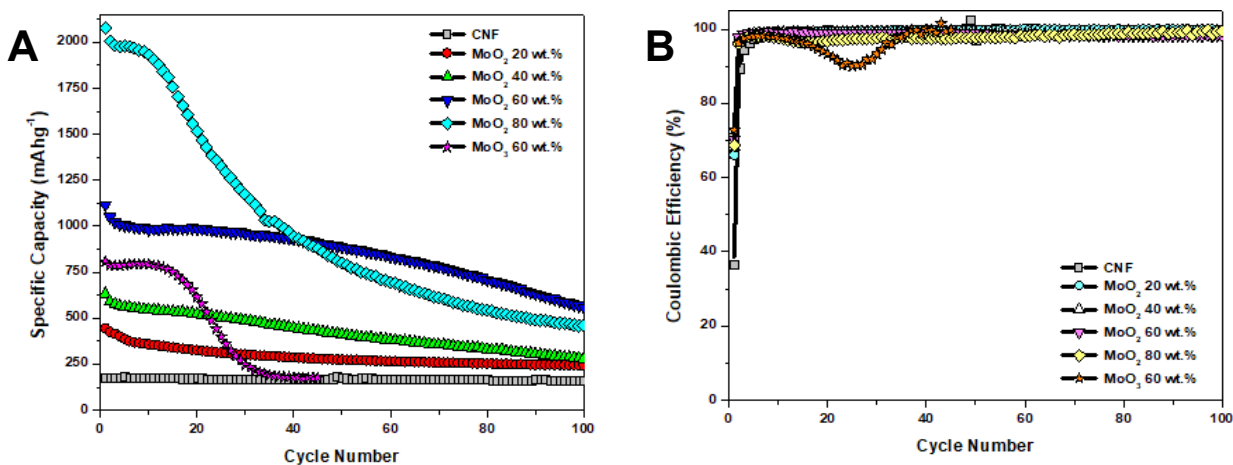


Figure 14. Cycle performance and coulombic efficiency MoO_2/C and MoO_3/C composites

The galvanostatic charge-discharge performance on the MoO_2/C and MoO_3/C composite electrodes were done in a potential window between 0.05-3.00 V (vs. Li/Li^+) at a current density of 100 mA g^{-1} over 100 cycles (Figure 13 A, B). The voltage vs capacity curves agree with the CV analysis in Figure 13. The 1st discharge of the MoO_2/C and MoO_3/C composites revealed three plateaus at 1.71-1.44V, 1.44-1.28V, 1.28-0.01V, which are associated with the reduction peaks (lithiation) giving an initial capacity of 1590.58 and 1173.91 mAh g^{-1} , respectively. During the 1st charge, two potential plateaus at 1.68 and 1.41 V associated with the oxidation peaks (delithiation)

give an initial charge capacity of 1115.08 and 866.14 mAhg⁻¹. An irreversible loss of 30 and 26% transpired during the 1st discharge cycle that is credited with the SEI layer. Capacities increments, or activation processes, for MoO₂/C and MoO₃/C composites is commonly view in transition metal oxides attributed to crystalline defects. Other factors include a reversible formation of the SEI layer due to this event starting from the low voltage region. As subsequent cycles progress, the potential plateaus begin to fade away corresponding to partial aggregation of the pulverize material producing volume expansion but still preserve a charge cycle capacity of 557 mAhg⁻¹ after 100 cycles. The cyclic stability behavior of the CNF, MoO₂/C and MoO₃/C composite electrodes at 100 mAg⁻¹ is summarized in Figure 14A, while Figure 14B shows Coulombic efficiency over 100 cycles. The results in Figure 14A demonstrate that with gradual increments of MoO₂, the electrode begins to become more unstable at initial cycles while exhibiting a clear representation of the activation process. The MoO₂/C (20 wt.%) exhibited stable patterns to that of CNF but delivering a reversible capacity of only 231 mAhg⁻¹ after 100 cycles. The instability of the electrode began to shift as the content of MoO₂ rose beginning with MoO₂/C (40 wt.%) exhibiting an initial charge capacity of 631 mAhg⁻¹ that concluded at 278 mAhg⁻¹. The MoO₂/C (60 wt.%) manifested charge capacity retention of up to 557 mAhg⁻¹, having 66% retention of theoretical performance. The results in Figure 14B showed an initial Coulombic efficiency of 68-75% for MoO₂/C (40, 60,80 wt.%) which was then maintained at 99% of that capacity after the 5th cycle. The MoO₂/C (20 wt.%) simulated the CNF once again starting at 58%, where CNF began at 36% which can be attributed to the high surface area.

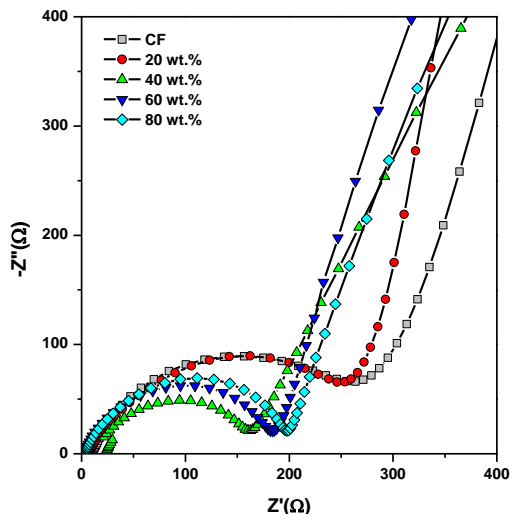


Figure 15. EIS measurements on various weight of MoO_2/C composites.

Electrochemical impedance spectroscopy (EIS) measurements were conducted in Li-ion half cells at an open-circuit voltage to further gain insight into the kinetics and electrochemical performance of the CF and MoO_2/C composite electrodes. Nyquist plots behavior of the fresh various ratios of the MoO_2/C and CF anode electrodes ran at a frequency range of 0.01 Hz to 100 kHz are shown in Figure 15. The simplified equivalent circuit model assists in clarifying the measurement results. The Nyquist plot are assembled of three components: the solution resistance (R_s) located at high frequencies, the charge transfer resistance (R_{CT}) corresponding to the diameter of the semicircle and the Warburg impedance (W) related to Li^+ diffusion in the solid state visualized by the straight line. Convincingly, comparable semicircle diameters occurring within the electrolyte and electrode interface to more excessive concentration (40 wt.%, 60 wt.%, 80 wt.%), insinuates low contact and charge transfer impedance at initial cycles.

Electrode	R_s (Ω)	R_{CT} (Ω)
CF	9.71	290
MoO ₃ /C	3.66	199
MoO ₂ /C	20 wt.%	6.36
	40 wt.%	10.8
	60 wt.%	2.62
	80 wt.%	3.99

Table 1. Impedance parameters values from the equivalent circuit model

Table 1 list the parameters of the equivalent circuit for the CF and MoO₂/C composites after fitting the diameter of the semicircle curves. The CF and 20 wt.% denote resistances in R_s (9.71 Ω and 290 Ω) and R_{CT} (6.36 Ω and 301 Ω). The uncomplete semi-circle indicates a deviation from the ideal circuit associated with diffusive processes. The 40 wt.% MoO₂/C electrode exhibits a significant reduced resistance in R_s (10.8 Ω) and R_{CT} (168 Ω), compared to that of CF. The 60 wt.% and 80 wt.% concentrations followed closely by (2.62 Ω and 191 Ω) and (3.99 Ω and 203 Ω), respectively. These high-middle frequency regions reduce semicircles from the EIS results implies that the incorporation of high MoO₂ concentrations enhances the conductivity, further improving the electrochemical performance.

4.2.2 MoS₂/GO AND MoS₂/RGO COMPOSITE ANODES

To understand the interaction process of Li⁺ with the MoS₂, hybrid MoS₂/GO and MoS₂/rGO composites, cyclic voltammetry (CV) measurements for the initial four cycles potential window ranging between 0.05-3.0 V (vs Li⁺/Li) at a scan rate of 0.2 mVs⁻¹ were conducted as shown in Figure 16. The first sharp reduction peak observed at ~ 1.1 V in the cathodic scan (lithiation) is associated with formation of Li_xMoS₂ by Li⁺ intercalation into the MoS₂ lattice (Eq. 1) including a phase transition of trigonal prismatic to octahedral structure. A follow-up reduction

peak observed at ~0.5 V which is assigned to the conversion of MoS₂ to Mo particles embedded in the Li₂S matrix (Eq. 2). In the anodic scan (delithiation), two peaks are observed at 1.65 and 2.25 V are attributed to the partial oxidation of Mo to MoS₂ and to the extraction of Li₂S and oxidation of LiS₂ into sulfur (S) or polysulfides. The peak at 1.5-1.85 and 1.25 V shown in subsequent cathodic sweep partakes a conversion of S to Li₂S and Li⁺ intercalation (Eq. 3) [46]. The three reaction mechanisms dependent on the structure of the metal sulfide can be seen below:

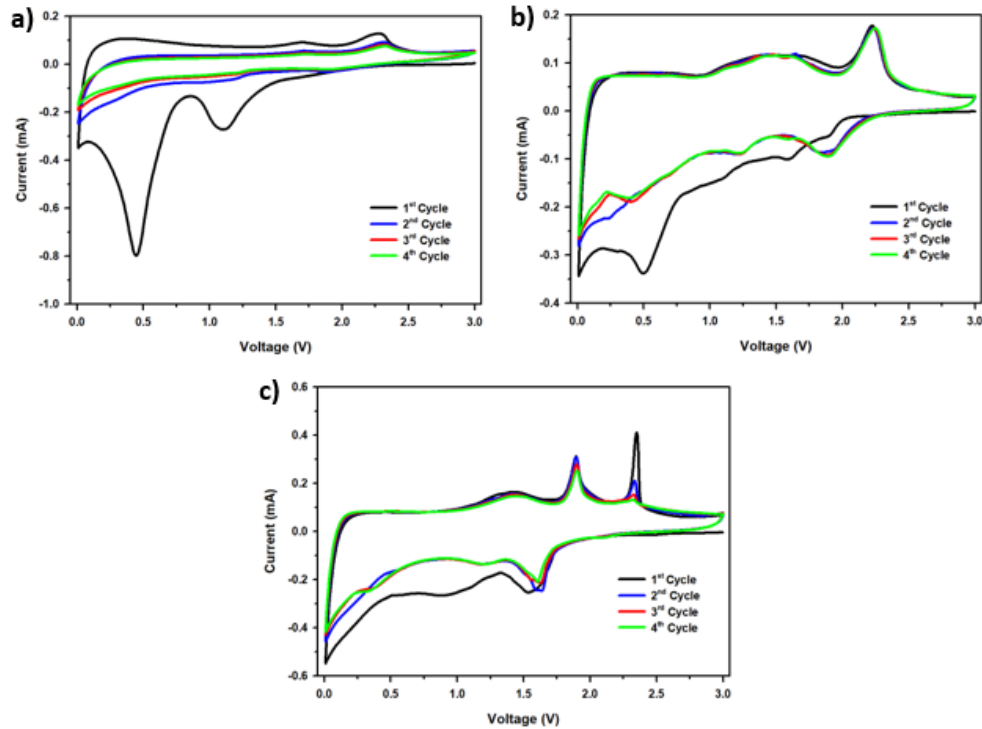
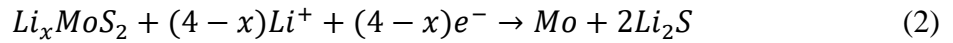


Figure 16. CV curves of (a) mos₂, (b) hybrid mos₂/go, and (c) mos₂/rgo composites.

The galvanostatic charge-discharge performance of hybrid MoS₂/GO and MoS₂/GO composite electrodes was done in a potential window ranging between 0.05-3.0V (vs Li⁺/Li) at a current density of 100 mA g⁻¹ over 100 cycles (Figure 17a,b), where the voltage vs. capacity curves can be identified correlating with the CV analysis in Figure 16. The 1st discharge for the hybrid MoS₂/GO and MoS₂/GO reveals three plateaus at 1.7-1.6V, 1.6-0.71V, 0.71-0.01V correlate with the reduction reactions occurring during lithiation giving an initial capacity of 980 and 1068 mAhg⁻¹, respectively. During the charge (delithiation) process, two potential plateaus located at 2.3V, which loosen from the initial sharpened peak, and 1.88V also agree with the previous CV curves. In both the cases, an initial charge capacity resemblance is seen of 640 mAhg⁻¹, indicating an irreversible capacity loss of 35 and 40% in the 1st discharge capacity highly attributed to the formation of the solid electrolyte interface (SEI) layer. Ultimately, the hybrid MoS₂/rGO and MoS₂/GO composites showed a 100th charge cycle capacity of 561 and 504 mAhg⁻¹, respectively, corresponding to a plane reduction in charge capacity retention of 87 and 79% from the 1st cycle. Figure 18(a, c) reiterates the cyclic stability behavior of the MoS₂/GO and MoS₂/GO composite electrodes at 100 mA g⁻¹ in the same potential range during the charge cycle performance, while Figure 18(b, d) shows Coulombic efficiency over 100 cycles for diverse weight ratios of MoS₂ and GO. MoS₂/GO (Figure 18a) shows in such a way that after the initial 40 cycles, a slight reduction on the specific capacity to 516 mAhg⁻¹ transpires before manifesting excellent capacity retention up to 505 mAhg⁻¹ for 6.5:1 after 100 cycles. Additionally, MoS₂/GO (1:1) and MoS₂/GO (2:1) hybrids exhibited patterns to that of MoS₂/GO (6.5:1), but its reversible capacities were only 290 and 354 mAhg⁻¹ after 100 cycles, respectively. In contrast, MoS₂/rGO (1:1), MoS₂/rGO (2:1) and MoS₂/rGO (6.5:1) hybrid composites exhibited significant improved cycling performance of 411, 474 and 561 mAhg⁻¹ after 100 cycles (Figure 18c). Figure 18(b,d) demonstrates an initial

Coulombic efficiency (CE) of 61-67% for all MoS₂/GO and MoS₂/rGO composites, which was then maintaining ~99% of that capacity after the 5th cycle. Moreover, the charge capacity of MoS₂/rGO (6.5:1) gradually increases from 516 to 561 mAhg⁻¹ after the 15th cycle experiencing an activated process resulting from partial MoS₂ failing to react with Li⁺ after initial cycles providing continuous rapid linear kinetics even after 100 cycles. This can be supported by the trace of MoS₂ oxidation peaks coupled with intensive S reduction with ongoing cycles (Figure 16c).

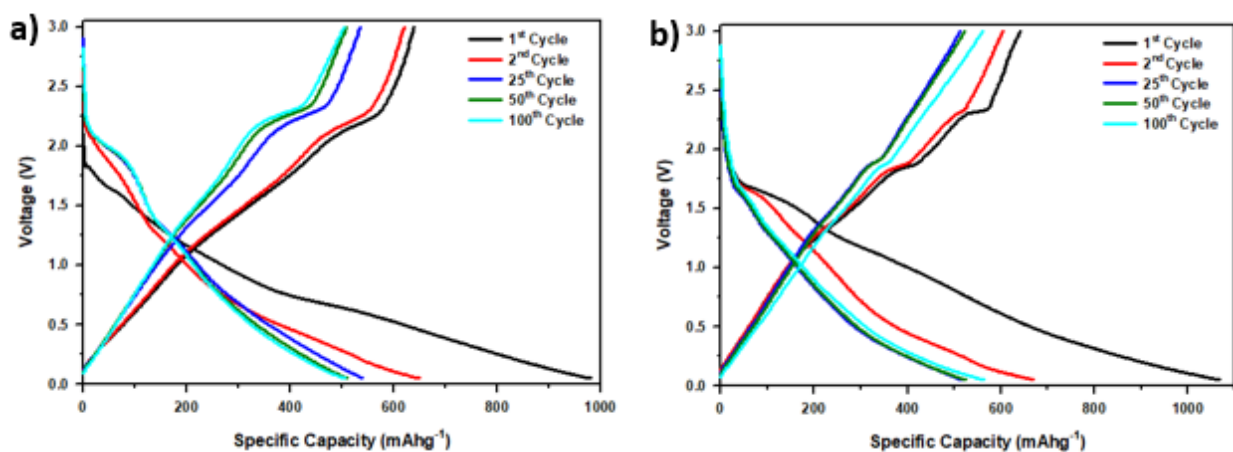


Figure 17. Charge-discharge performance of (a) MoS₂/GO and (b) MoS₂/rGO composites.

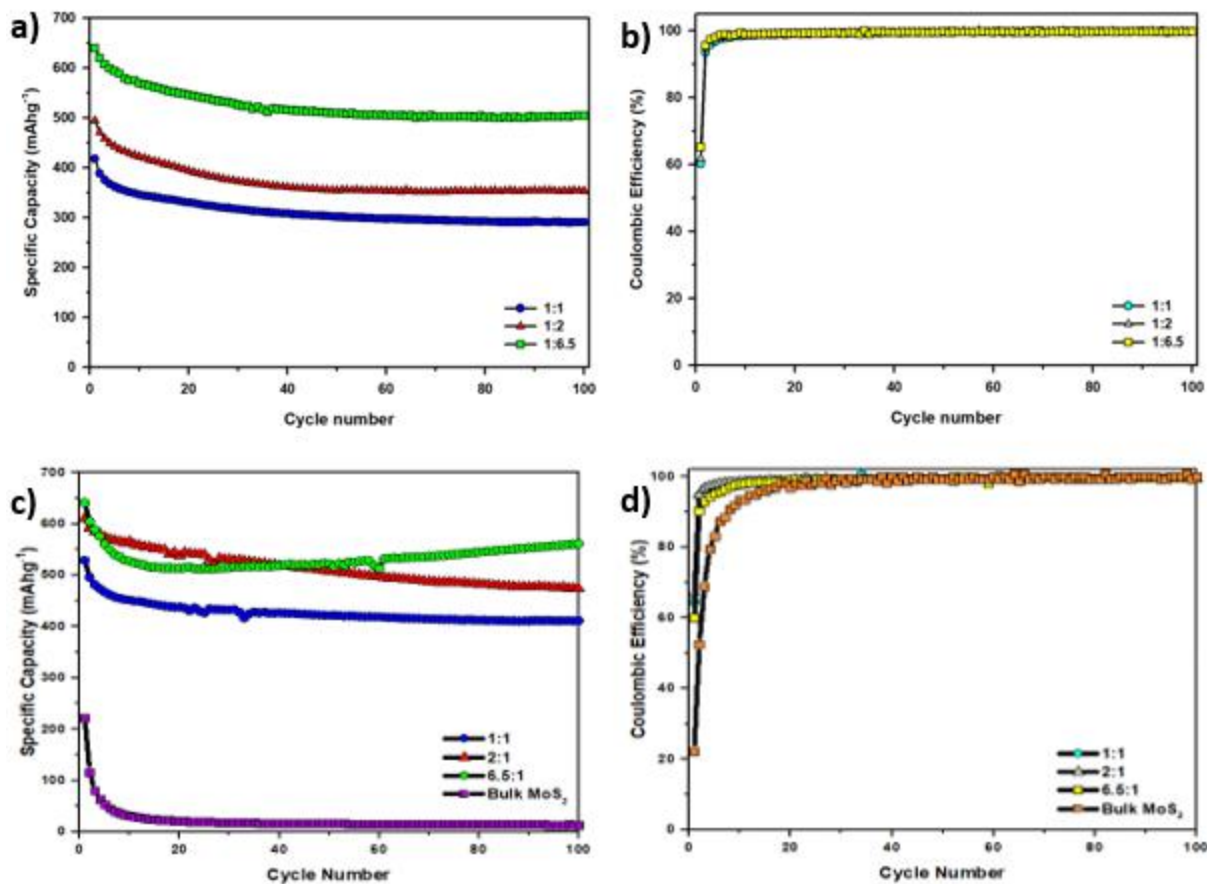


Figure 18. CP and coulombic efficiency on (a, b) MoS_2/GO and (c, d) MoS_2/rGO .

To better understand the kinetics and enhanced electrochemical performance of the various weight ratios of the hybrid composites, the electrochemical impedance spectroscopy (EIS) measurements of MoS_2/GO and MoS_2/GO at initial cycles are shown in Figure 19(a, b). The Nyquist spectra consist of a semicircle, involving the electrolyte solution resistance (R_s) and the charge transfer resistance (R_{CT}) between the electrode/electrolyte determine by the diameter at high-medium frequency region. [49] The slope of the straight line is inversely proportional to the Li^+ diffusion in the solid state is represented as Warburg impedance (W) and the constant phase-angle element (CPE) equivalent to the double layer capacitance. The measurements based on the fitting procedure indicate that the values for R_s for the (6.5:1) MoS_2/GO and (6.5:1) MoS_2/rGO

were determined to be 1.98 and 7.59 Ω , respectively, while the values for R_{CT} were 205 and 199 Ω . Visibly, MoS₂/rGO Nyquist spectrums for all weight ratios of MoS₂ and GO in Figure 19b exhibits small comparable diameters signifying supreme charge transfer kinetics. The reduction of GO permitted high conductivity allowing rapid electron and ion transport during charging-discharging cycles compared to the MoS₂/GO mixtures. Since, MoS₂/GO holds lower contact and charge-transfer resistance than MoS₂, the (1:1) hybrid composites experience the largest diameter within the semicircle, which lessens as the content of MoS₂ grew [60]. The present EIS results are in agreement with the cycle performance in Figure 18(a,b).

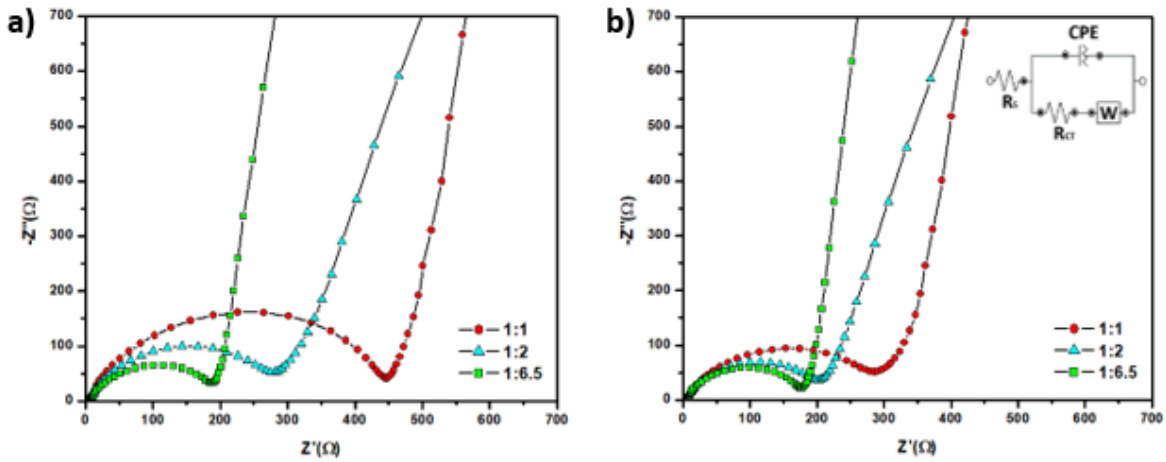


Figure 19. EIS of (a) mos₂/go and (b) mos₂/rgo.

Electrode		R_s (Ω)	R_{CT} (Ω)
MoS ₂ /GO	1:1	3.71	478
	1:2	6.44	311
	1:6.5	1.98	205
MoS ₂ /rGO	1:1	5.36	330
	1:2	3.65	219
	1:6.5	7.59	199

Table 2. EIS parameters values from the equivalent circuit model fitting.

CHAPTER V

CONCLUSION

The MoS₂/GO composites have been successfully synthesized through a modified hummer's method with varying concentrations of MoS₂ to GO. The calcination heat treatments of GO in air resulted in the carbon matrix being exfoliated while maintaining the MoS₂ anchor onto the surface, which were observed by the SEM studies. The MoS₂/rGO and MoS₂/GO composites avoided the restacking and aggregation that bulk MoS₂ is well identified for, maintaining a high conductive median facilitating the kinetics hence improving the electrochemical performance for the hybrid electrodes. The notable activation process which occurred during the MoS₂/rGO derived 88% of its initial capacity to be retain after 100 cycles concluding at 561 mAhg⁻¹, from where the electrode began at a charge capacity of 641 mAhg⁻¹. The high reversible capacity of the MoS₂/rGO generated from MoS₂/GO may be considered as a candidate potential stable high-capacity anode for the next generation LIBs.

The reciprocal production of MoO₂/C and MoO₃/C has been performed through the centrifugal spinning of precursor solutions and subsequent heat treatment. The MoO₃ electrode, as a LIB anode material, exhibited a high reversible capacity of 836 mAhg⁻¹ at a current density of 100 mA_g-1 reaching ~75 % of its theoretical capacity. Furthermore, the MoO₂/C composite fibers experienced similar patterns to MoO₃ undergoing a rise in reversible

capacity after 10 cycles. Although, the 60 wt.% MoO₂/C composite fibers exhibit a specific capacity achieving of 526 mAhg⁻¹, after 100 cycles, further work revolves around is needed to improve the electrochemical performance.

CHAPTER VI

FUTURE WORK

Future work on this thesis involves conducting further test with higher current densities with the ceramic composites involving rGO. Rate performance can be implemented to view the activation mechanisms of the MoS₂ with and exploring the conductive carbon-based material with the molybdenum oxides. With the 50% capacity retention made with the carbon fibers at 60% concentration, the addition of rGO embedded within the CFs could allow for further modifications of the morphology minimizing mechanical stresses due to volume expansion experience during the prolonged cycles. The molybdenum oxides could be embedded within the CFs once again with TiO₂, as well as providing a porous structure with polymer blends such as PS and PMMA. The facile synthesis success of these materials can allow for further investigations with sodium-ion batteries as well.

REFERENCES

1. Bithas, K. and P. Kalimeris, A Brief History of Energy Use in Human Societies, in Revisiting the Energy-Development Link: Evidence from the 20th Century for Knowledge-based and Developing Economies. 2016, Springer International Publishing: Cham. p. 5-10.
2. Reddy, Mogalahalli V., et al. "Brief history of early lithium-battery development." *Materials* 13.8 (2020): 1884.
3. Diouf, Boucar, and Ramchandra Pode. "Potential of lithium-ion batteries in renewable energy." *Renewable Energy* 76 (2015): 375-380.
4. Blomgren, George E. "The development and future of lithium ion batteries." *Journal of The Electrochemical Society* 164.1 (2016): A5019.
5. Leuthner, Stephan. "Lithium-ion battery overview." *Lithium-Ion Batteries: Basics and Applications*. Springer, Berlin, Heidelberg, 2018. 13-19.
6. Berdichevsky, Gene, et al. "The tesla roadster battery system." *Tesla Motors* 1.5 (2006): 1-5.
7. Castelvechi, Davide. "Will Tesla's battery change the energy market?." *Nature News* (2015).
8. Uitz, M., et al. "Aging of tesla's 18650 lithium-ion cells: Correlating solid-electrolyte-interphase evolution with fading in capacity and power." *Journal of The Electrochemical Society* 164.14 (2017): A3503.
9. Pirani, S., Burning up: A global history of fossil fuel consumption. 2018: Pluto Press.
10. Li, M., et al., 30 years of lithium-ion batteries. *Advanced Materials*, 2018. 30(33): p. 1800561.
11. Zubi, G., et al., The lithium-ion battery: State of the art and future perspectives. *Renewable and Sustainable Energy Reviews*, 2018. 89: p. 292-308.

12. Oswal, Mehul, Jason Paul, and Runhua Zhao. "A comparative study of lithium-ion batteries." *University of southern California* (2010): 2419-2430.
13. An, Seong Jin, et al. "The state of understanding of the lithium-ion-battery graphite solid electrolyte interphase (SEI) and its relationship to formation cycling." *Carbon* 105 (2016): 52-76.
14. Yoshio, Masaki, et al. "Improvement of natural graphite as a lithium-ion battery anode material, from raw flake to carbon-coated sphere." *Journal of Materials Chemistry* 14.11 (2004): 1754-1758.
15. Kumar, T. Prem, T. Sri Devi Kumari, and Manuel A. Stephan. "Carbonaceous anode materials for lithium-ion batteries—the road ahead." *Journal of the Indian Institute of Science* 89.4 (2009): 393-424.
16. Chen, Haisheng, et al. "Progress in electrical energy storage system: A critical review." *Progress in natural science* 19.3 (2009): 291-312.
17. Korpaas, Magnus, Arne T. Holen, and Ragne Hildrum. "Operation and sizing of energy storage for wind power plants in a market system." *International Journal of Electrical Power & Energy Systems* 25.8 (2003): 599-606.
18. Hesse, Holger C., et al. "Lithium-ion battery storage for the grid—a review of stationary battery storage system design tailored for applications in modern power grids." *Energies* 10.12 (2017): 2107.
19. Hunt, Julian David, et al. "Mountain Gravity Energy Storage: A new solution for closing the gap between existing short-and long-term storage technologies." *Energy* 190 (2020): 116419.
20. Attonaty, Kévin, et al. "Thermodynamic and economic evaluation of an innovative electricity storage system based on thermal energy storage." *Renewable Energy* 150 (2020): 1030-1036.
21. None, None. *Energy Frontier Research Centers: Science For Our Nation's Energy Future* (July 2019). USDOE Office of Science (SC), Washington, DC (United States), 2019.
22. Yoshio, Masaki, Ralph J. Brodd, and Akiya Kozawa. *Lithium-ion batteries*. Vol. 1. New York: Springer, 2009.
23. Kushwaha, Anoop Kumar, et al. "Engineering redox potential of lithium clusters for electrode material in lithium-ion batteries." *Journal of Cluster Science* 28.5 (2017): 2779-2793.

24. Feng, Xuning, et al. "Thermal runaway mechanism of lithium ion battery for electric vehicles: A review." *Energy Storage Materials* 10 (2018): 246-267.
25. A. k. Covington, *Physical chemistry of organic solvent systems*, Springer Science & Business Media, 2012.
26. Zhu, Taohe, et al. "Manipulating the Composition and Structure of Solid Electrolyte Interphase at Graphite Anode by Adjusting the Formation Condition." *Energy Technology* 7.9 (2019): 1900273.
27. Winter, Martin, et al. "Insertion electrode materials for rechargeable lithium batteries." *Advanced materials* 10.10 (1998): 725-763.
28. Béguin, F., et al. "Correlation of the irreversible lithium capacity with the active surface area of modified carbons." *Carbon* 43.10 (2005): 2160-2167.
29. Yoshio, Masaki, Ralph J. Brodd, and Akiya Kozawa. *Lithium-ion batteries*. Vol. 1. New York: Springer, 2009.
30. De las Casas, Charles, and Wenzhi Li. "A review of application of carbon nanotubes for lithium ion battery anode material." *Journal of Power Sources* 208 (2012): 74-85.
31. Mahmood, Nasir, Tianyu Tang, and Yanglong Hou. "Nanostructured anode materials for lithium ion batteries: progress, challenge and perspective." *Advanced Energy Materials* 6.17 (2016): 1600374.
32. Roy, Poulomi, and Suneel Kumar Srivastava. "Nanostructured anode materials for lithium ion batteries." *Journal of Materials Chemistry A* 3.6 (2015): 2454-2484.
33. Zhou, Xiaosi, Li-Jun Wan, and Yu-Guo Guo. "Binding SnO₂ nanocrystals in nitrogen-doped graphene sheets as anode materials for lithium-ion batteries." *Advanced materials* 25.15 (2013): 2152-2157.
34. Mahmood, Nasir, and Yanglong Hou. "Electrode Nanostructures in Lithium-Based Batteries." *Advanced Science* 1.1 (2014): 1400012.
35. Guo, Juchen, and Chunsheng Wang. "Nanostructured Metal Oxides for Li-Ion Batteries." *Functional Metal Oxide Nanostructures*. Springer, New York, NY, 2012. 337-363.
36. Ji, Liwen, et al. "Recent developments in nanostructured anode materials for rechargeable lithium-ion batteries." *Energy & Environmental Science* 4.8 (2011): 2682-2699.
37. Sen, Uttam Kumar, and Sagar Mitra. "Synthesis of molybdenum oxides and their electrochemical properties against Li." *Energy Procedia* 54 (2014): 740-747.

38. Hu, X., et al., Nanostructured Mo-based electrode materials for electrochemical energy storage. *Chemical Society Reviews*, 2015. 44(8): p. 2376-2404.
39. Zhou, X.-h., et al., General construction of molybdenum-based compounds embedded in flexible 3D interconnected porous carbon nanofibers with protective porous shell for high-performance lithium-ion battery. *Carbon*, 2021. 179: p. 142-150.
40. Yu, S.-H., et al., Understanding Conversion-Type Electrodes for Lithium Rechargeable Batteries. *Accounts of Chemical Research*, 2018. 51(2): p. 273-281.
41. Lu, Y., L. Yu, and X.W. Lou, Nanostructured Conversion-type Anode Materials for Advanced Lithium-Ion Batteries. *Chem*, 2018. 4(5): p. 972-996.
42. Ette, P.M., P. Gurunathan, and K. Ramesha, Self-assembled lamellar alpha-molybdenum trioxide as high performing anode material for lithium-ion batteries. *Journal of Power Sources*, 2015. 278: p. 630-638.
43. Sen, U.K. and S. Mitra, Synthesis of Molybdenum Oxides and their Electrochemical Properties against Li. *Energy Procedia*, 2014. 54: p. 740-747.
44. Thapaliya, B.P., et al., Synthesizing High-Capacity Oxyfluoride Conversion Anodes by Direct Fluorination of Molybdenum Dioxide (MoO₂). *ChemSusChem*, 2020. 13(15): p. 3825-3834.
45. Wu, D., et al., Mixed Molybdenum Oxides with Superior Performances as an Advanced Anode Material for Lithium-Ion Batteries. *Scientific Reports*, 2017. 7(1): p. 44697.
46. Stephenson, T., et al., Lithium ion battery applications of molybdenum disulfide (MoS₂) nanocomposites. *Energy & Environmental Science*, 2014. 7(1): p. 209-231.
47. Zhang, X., et al., Synthesis of MoS₂@C Nanotubes Via the Kirkendall Effect with Enhanced Electrochemical Performance for Lithium Ion and Sodium Ion Batteries. *Small*, 2016. 12(18): p. 2484-2491.
48. Hu, S., et al., Facile and Green Preparation for the Formation of MoO₂-GO Composites as Anode Material for Lithium-Ion Batteries. *The Journal of Physical Chemistry C*, 2014. 118(43): p. 24890-24897.
49. Palanisamy, K., et al., Self-assembled porous MoO₂/graphene microspheres towards high performance anodes for lithium ion batteries. *Journal of Power Sources*, 2015. 275: p. 351-361.

50. Xie, S., et al., Coaxially Integrating TiO₂/MoO₃ into Carbon Nanofibers via Electrospinning towards Enhanced Lithium Ion Storage Performance. *ChemistrySelect*, 2020. 5(11): p. 3225-3233.
51. Chen, C., et al., Chemical vapor deposited MoS₂/electrospun carbon nanofiber composite as anode material for high-performance sodium-ion batteries. *Electrochimica Acta*, 2016. 222: p. 1751-1760.
52. Zeng, L., et al., An ultra-small few-layer MoS₂-hierarchical porous carbon fiber composite obtained via nanocasting synthesis for sodium-ion battery anodes with excellent long-term cycling performance. *Dalton Transactions*, 2019. 48(13): p. 4149-4156.
53. Zhang, M., et al., Nanocasting and Direct Synthesis Strategies for Mesoporous Carbons as Supercapacitor Electrodes. *Chemistry of Materials*, 2018. 30(21): p. 7391-7412.
54. Li, W., et al., Nanostructured electrode materials for lithium-ion and sodium-ion batteries via electrospinning. *Science China Materials*, 2016. 59(4): p. 287-321.
55. Shi, X., et al., Electrospinning of nanofibers and their applications for energy devices. *Journal of Nanomaterials*, 2015. 2015.
56. Pampal, E.S., et al., A review of nanofibrous structures in lithium ion batteries. *Journal of Power Sources*, 2015. 300: p. 199-215.
57. Sarkar, K., et al., Electrospinning to forcespinning™. *Materials today*, 2010. 13(11): p. 12-14.
58. Zhao, C., et al., Self-assembly-induced alternately stacked single-layer MoS₂ and N-doped graphene: A novel van der Waals heterostructure for lithium-ion batteries. *ACS applied materials & interfaces*, 2016. 8(3): p. 2372-2379.
59. Loo, Adeline Huiling, et al. "Exfoliated transition metal dichalcogenides (MoS₂, MoSe₂, WS₂, WSe₂): an electrochemical impedance spectroscopic investigation." *Electrochemistry Communications* 50 (2015): 39-42.
60. Li, Honglin, et al. "MoS₂/graphene hybrid nanoflowers with enhanced electrochemical performances as anode for lithium-ion batteries." *The Journal of Physical Chemistry C* 119.14 (2015): 7959-7968.

APPENDIX

State-of-the-Art Methods

METHOD	EQUIPMENT	PURPOSE	RESULTS OBTAINED
Characterization	Scanning Electron Microscope (SEM)	Microscope to measure fiber diameter, particle size and observe the morphology of the fibers/synthesized active material	Molybdenum-based materials (MoO ₃ , MoO ₃ /TiO ₂ , MoS ₂ , MoS ₂ /GO, MoS ₂ /rGO, MoO ₂ /C, MoO ₂ /TiO ₂ /C) focused on morphologies, as well as fiber diameters and particle size. The Mo-sulfides demonstrated desired few layer and multi-layer, while influencing carbonaceous composites (GO reducing to rGO). The MoO ₂ /C succeeded in fabrication of high content material having the carbon buffer the volume change. The fibers were oxidized to produced synthesized MoO ₃ and MoO ₃ /TiO ₂ material.
	Energy-dispersive X-ray spectroscopy (EDS, EDX)	Elemental analysis used to characterize carbonized fibers with embedded active material content and synthesized active material.	Results showed Mo-based materials introduced to carbon fibers demonstrated high levels of content maintain throughout the fabrication process.
	Thermogravimetric Analysis (TGA)	Measure changes in mass as a function of temperature in air atmosphere to obtain active	Another analysis to observe the active material content following EDS. Confirmation of the desired active material content was kept through the fabrication process.

		material content with respect to carbon, analyzed the oxidation reactions occurring.	
	Transmission Electron Microscope (TEM)	Instrument for structural and chemical characterization at the nanoscale for synthesized fibers	Further analysis to observe the active material content following EDS and TGA. Confirmation of the desired active material content was kept through the fabrication process.
	Differential Scanning Calorimetry (DSC)	Measured how physical properties of green fiber samples change, along with temperature against time.	The results were further used to calculate the specific heat capacity of the precursor polymer PAN fibers using a procedure found in literature. This was also done to determine the thermal stability of the TiS ₂ /PAN composite. The paper was published as Centrifugally spun TiO ₂ /C composite fibers prepared from TiS ₂ /PAN precursor fibers as binder-free anodes for LIBS.
	X-ray photoelectron spectroscopy (XPS)	Technique use to analyze the surface chemistry of the synthesized active material.	Results demonstrated that GO did reduced to rGO through a calcination heat treatment when temperature went from 450 °C to 550 °C.
	X-ray diffraction (XRD)	Technique used to characterize the crystal structure, phase, and other structural parameters for confirmation of the desired active	Results demonstrated the proper synthesis of the Mo-based materials.

Characterization		material that was synthesized.	
Battery Fabrication and Testing	Force spinning	Fabricate fibers.	Multiple fiber mats used to produce carbon fiber anodes with active materials.
	OTF-1200X	Heat treatment of fibers.	Fabricated fibers went through a heat treatment. The program was based on both the polymer and active material.
	MBRAUN Glovebox	Controlling environment during battery assembly process.	Production of multiple LIB batteries in inert gas due to Li chip utilized as a cathode being highly reactive if the cell is assembled under air.
	LANHE Battery Testing System	Battery cycler analyzing the cycle life by the number of charge and discharge profiles completed over time (CP).	Results demonstrated that Mo-based materials as anode electrodes have potential to be commercially utilized due to data having utmost influential performance after prolonged cycles.
	BioLogic Science Instrument	Battery cycler focus on cyclic voltammetry (CV) analyzing the resulting current derived by cycling the potential of a working electrode.	Results demonstrated proper REDOX reactions with all Mo-based materials aligned with literature. The subsequent cycles demonstrated reversibility and stability over time.
	Arbin Instrument	Battery cycler focus on	Results demonstrated high performance of Mo-based materials

		analyzing performance of the cell with increasing rate (RP).	can be achieve with increasing rates, however the materials the aid of titanium oxide or carbonaceous composites are required to prolong and stabilize the high performance.
	AUTOLAB	This battery tester is focus on the electrochemical impedance spectroscopy (EIS) of the cell. measuring the impedance of a system in dependance of the AC potential frequency.	Results focus on analyzing the resistance to ion transport and the rate of ions diffusion.
	LANDdt	CP	Performance evaluation done over a voltage range of 0.01-3.00 V vs. Li/Li ⁺ . Set up number of cycles, current density, rest/non-rest cycling, as well as formation cycles meaning slowing rate at the first cycle for the LANHE Battery Testing System.
	MITS Pro	RP	Performance evaluation done over a voltage range of 0.01-3.00 V vs. Li/Li ⁺ with different current densities for Arbin Instrument.
	NOVA	CV	Performance evaluation done over a scan rate of 0.1 mVs ⁻¹ ranging between 0.05 and 3.00 V for BioLogic Science Instrument.
	BT LAB	EIS	Measurement done over a frequency range from 1 kHz and 0.005 Hz for AUTOLAB.
	ImageJ	Used for Histograms based	Utilize histograms to consider the diameter size distribution of the

Software		on SEM images (Typically 2 or 3 images required)	fibers being manufactured in the research lab through force spinning.
	SIGMAPLOT	Plotting characterization and electrochemical data.	CV, CP, RP, and EIS were plotted and added for upcoming publication.
	ORIGIN	Plotting characterization and electrochemical data.	CV, CP, RP, and EIS were plotted and added for upcoming publication.
	EndNote	Managing and sorting citations.	Managing and sorting citations for upcoming publication.
	Microsoft Office (Word, Power Point, Excel), Notepad	Writing research paper/thesis, thesis presentation material, transferring and organizing data.	Managing and sorting finalize plotted CV, CP, RP, EIS, and additional schematics which were used for upcoming publication.

BIOGRAPHICAL SKETCH

Ramiro Gonzalez Jr. was born in Weslaco, TX to Maria Gonzalez and Ramiro Gonzalez. He lived in Mexico for six years until he moved to Edinburg, TX and has been living there since then. He started elementary school at Lincoln Elementary and then transitioned to Barrientes Middle School. Ramiro graduated from J. Economedes High School landing at top 10%. During his years in High School, he had a passion for math and science he got certified in CPR, since he wanted to pursue nursing. After graduation he enrolled in the University of Texas Rio Grande Valley where he started off with a Civil Engineering degree. After a year in he decided to pursue Mechanical Engineering where Ramiro knew it would be a career that open doors that would eventually help him provide for himself and his family. He graduated with a Bachelor's degree in Mechanical Engineer and a Masters in Mechanical Engineering. Before graduating, he was given the opportunity join Dr.Alcoutlabi's research lab. He has been researching rechargeable lithium-ion batteries for 4 years. After graduation, Ramiro hopes to continue working in the field of electrochemistry. He can be contacted at jr.ramirogonzalez02@gmail.com.